Epitaxial Silicon Growth Rate Control

by

Safroadu Kwadwo Yeboah-Amankwah

S.B., Massachusetts Institute of Technology (1993)

Submitted to the Department of Electrical Engineering and Computer Science
in partial fulfillment of the requirements for the degree of

Master of Engineering in Electrical Engineering

at the

MASSACHUSETTS INSTITUTE OF TECHNOLOGY

May 1994

Author .....
Department of Electrical Engineering and Computer Science
May 18, 1994

Certified by .....
Duane S. Boning
Assistant Professor of Electrical Engineering
Thesis Supervisor

Accepted by .....
Frederic R. Morgenthaler
Chairman, Departmental Committee on Graduate Students

Epitaxial Silicon Growth Rate Control

by

Safroadu Kwadwo Yeboah-Amankwah

Submitted to the Department of Electrical Engineering and Computer Science
on May 18, 1994, in partial fulfillment of the
requirements for the degree of
Master of Engineering in Electrical Engineering

Abstract

In this thesis a multi-loop controller for epitaxial silicon deposition in an Ultra High Vacuum reactor is designed and built. The process is constrained to the low pressure and low temperature regime. An Emission Fourier Transform Infrared Spectroscopy (EFT-IR) *in-situ* sensor for thickness measurements together with temperature sensors are used to monitor the state of the process for control. The ultimate goal of the controller is to maintain a constant desired growth rate of the epi-silicon given the limitations of the sensors.

Using experimental results a theoretical model for the process is developed and compared to previously reported results. A number of issues are addressed in the design and implementation of the controller. First, thickness measurements from the EFTIR are only available at finite time points during the course of the run; thickness measurements are generated once every 40–45 seconds. Along with the time delay, there is significant noise associated with this measurement, and quantization also presents a problem. Furthermore, the measurement of system variables such as temperature and pressure are particularly prone to system and measurement noise. Finally, non-linearities are present in some of the state sensors.

To address these issues, and to take maximum advantage of the available environment and wafer state sensors, a hierarchical structure is adopted for the real-time controller. An inner control loop maintains a desired process environment (temperature). An outer adaptive control loop achieves and maintains a desired change in wafer state (epitaxial silicon growth rate) based on *in-situ* thickness measurements and the growth model.

Dramatic improvements in reaching thermal set points are attained by the inner-loop controller. However, quantization of the thickness measurements impose a limitation on the speed and effectiveness of the outer loop. Possible improvements and suggested future work are included.

Thesis Supervisor: Duane S. Boning
Title: Assistant Professor of Electrical Engineering

Acknowledgments

I would like to thank those people who have made this project possible. My research advisor, Dr. D. Boning, who guided this work, providing valuable assistance and insight into this work. I am also very grateful for his encouragement and time along the way. Dr. Zhen Zhou who presided over most laboratory work for this thesis. I will like to thank Zhen for his patients, time and for guidance in the Microsystems Technology Laboratory (MTL). Weize Chen, Hyoun-Woo Kim and Rajan Naik for their assistance in the laboratory. I will like to thank them for their patience and time.

To my parents, Rose and David Yeboah-Amankwah, special thanks them for their endearing support and strength. To my siblings, Nana and Asuama, for making the effort worthwhile. To my host parents, Gwen and Cici Adu-Gyemfi, for their advice and encouragement. To my friends: Graham Fernandes, John Gachora, Ekundayo Okunyemi, Dennis Ouma, Lerato Setshwaelo, Sridhar Venkatesh and Robert Wickham. I thank them for the companionship during those late nights and early mornings and for making it all worth it. Thanks for all the memories.

Special thanks go to MTL for giving me access to the necessary experimental facilities. I will also like to thank ARPA under contract N00174-93-C-0035 for support for this project.

Contents

1 Introduction **9**

1.1 Objective 9

1.2 Background and Previous Work 10

1.3 Work Outline 11

2 Epitaxial Growth Model **13**

2.1 Introduction 13

2.2 Model Development 13

2.3 Factors Affecting Model Parameters 15

2.4 Model Parameters 17

2.5 Sensitivity 19

2.6 Control 20

3 Design and Implementation of the Temperature Loop Controller **21**

3.1 Introduction 21

3.2 Reactor and Control System 22

3.2.1 Heating System 23

3.2.2 Temperature Sensing 23

3.2.3 Temperature Model 26

3.3 Controller Design 27

3.3.1 Compensator Design 28

3.4 Practical Issues 31

3.5 Results 32

4 Design and Implementation of the Outer Loop Controller **37**

4.1 Introduction 37

4.2 Controller Design 38

4.3 Controllers 40

4.3.1 Linearised Model Update 40

4.3.2 Adaptive Controller - Pre-exponential 41

4.3.3 Adaptive Controller - Pre-exponential and Activation Energy . 42

4.4 Simulations 43

4.4.1 Linearised Model Update 44

4.4.2 Adaptive Controller - Pre-exponential 46

4.4.3 Adaptive Controller - Pre-exponential and Activation Energy . 47

4.5 Quantization 47

5 Conclusion **57**

5.1 Summary 57

5.2 Future Work 58

A The Kalman Filter **59**

A.0.1 The system 59

A.0.2 The Filter 60

B Simulation Blocks **61**

C Controller Interface **63**

D Hardware Setup (UHV Reactor and Computer Controller) **64**

List of Figures

1-1 Measurements of epitaxial film thickness for two different temperatures. 11

2-1 Epitaxial film growth under different initial cleaning conditions 16

2-2 *In-situ* thickness measurements for various growth conditions. 17

2-3 Growth rate of model with changing temperature and pressure. . . . 19

3-1 The LPCVD epitaxial reactor schematic. 22

3-2 Wiring schematic of heater power supply. 24

3-3 Optical sensor measurements for a constant wafer temperature. . . . 25

3-4 Thermo-couple measurements for a constant wafer temperature. . . . 25

3-5 Heater drive voltage versus steady state system temperature. 27

3-6 Heating and cooling time constants; response to a step voltage change is shown. 28

3-7 Sampled Bode Plot of System 29

3-8 Bode plot of open loop simple gain compensated system. 30

3-9 Bode plot of open loop pole-zero compensated system. 31

3-10 Bode plot of open loop PID compensated system. 32

3-11 Temperature and voltage measurements during step change in desired temperature set-point under simple gain compensation. 33

3-12 Temperature and voltage measurements during step change in desired temperature set-point under PZ compensation. 34

3-13 Temperature and voltage measurements during step change in desired temperature set-point under PID compensation. 35

3-14 EFTIR thickness measurements under PID controlled temperature. . 36

4-1 The hierarchical controller flowchart. 38
4-2 Linear outer loop control procedure. 41
4-3 Adaptive procedure for pre-exponential constant based control. 42
4-4 The Block Diagram for Type I System 45
4-5 Linear type I simulations - ΔT 46
4-6 Linear type I simulations - growth rate (microns/minute) 49
4-7 Linear type I simulations - desired temperature (^{o}C). 49
4-8 Linear type 0 simulation block diagram 50
4-9 Linear type 0 simulations - ΔT. 50
4-10 Linear type 0 simulations - growth rate (microns/minutes). 51
4-11 Linear type 0 simulations - desired temperature (^{o}C). 51
4-12 The adaptive controller simulation structure - pre-exp. 52
4-13 Adaptive pre-exp. simulations - temperature set-point (^{o}C). 52
4-14 Adaptive pre-exp. simulations - growth rate (microns/minute). 53
4-15 Adaptive Pre-exp. simulations - the pre-exponential coefficient. . . . 53
4-16 Simulation structure for adaptive control of pre-exp. and activation energy parameters. 54
4-17 Values for activation energy parameter during adaptive control simulation (cal/mole). 54
4-18 Values for pre-exponential parameter during adaptive control simulation. 55
4-19 Growth rate of system during adaptive controlled simulation (microns/minute). 55
4-20 Temperature set-point to inner loop during adaptive controlled simulations (K). 56

B-1 Inner temperature toop block for outer loop simulations. 61
B-2 Growth model for outer loop simulations. 62

List of Tables

2.1 Growth rate measurements for various growth conditions. 18

Chapter 1

Introduction

The growth of the semiconductor industry has demanded improvements in the acceptable accuracy as well as flexibility of processing steps. Manual and open loop set-point operations are giving way to systems with greater automation and control. Through *in-situ* sensors, state information about the processing step can be obtained, which in turn, can be used to compensate observed deviations from optimum performance. The use of *in-situ* sensors in real time allows for complex non-linear characteristics of processes to be feasibly modeled. Control parameters can then be updated in real time to account for these non-idealities in such complex, non-linear processes.

The ultimate goal of fine real time control for accurate and repeatable semiconductor manufacturing is limited by two factors. The overall controller ultimately relies on the accuracy of the *in-situ* sensors used to measure state parameters of the process for input to the controller. *In-situ* measurements are often of relatively poor quality with low signal-to-noise ratios compared to *ex-situ* measurements. Secondly, for good performance an accurate model (often non-linear) of the process being controlled must be derived for the appropriate operating regime.

1.1 Objective

The objective of this work was to design and build a real time growth rate controller for the epitaxial deposition of silicon. The work focussed on an Ultra High Vacuum

(UHV) reactor operating under low pressure and low temperature conditions. Using experimental results an improved theoretical model for the process was derived for use in the controller. An Emission Fourier Transfer Infrared (EFTIR) *in-situ* sensor for thickness measurements together with temperature sensors were used to design and implement a feedback controller for the epitaxial system. The ultimate goal of the controller was to maintain a constant desired growth rate of the epi-silicon given the limitations of the sensors and system.

1.2 Background and Previous Work

The work was performed using an ultra high vacuum single-wafer chemical vapour deposition reactor [1]. The reactor was operated in the low temperature regime, approximately less than 650°C using pure silane as the only reactant. The EFTIR sensor functions correctly only under these conditions. These conditions restrict the epitaxial deposition of silicon to be surface reaction limited. Of the four stage chemical process which characterize the incorporation of silicon atoms into surface sites, the critical one is the last [2]

$$2SiH^* \Longrightarrow 2^* + film + 2H \tag{1.1}$$

where * represents a surface site. For this limit, the growth rate, G [atoms/cm^{2}sec] is

$$G = \frac{Nk_d}{3} \tag{1.2}$$

where N is the number of surface sites, and k_d is the hydrogen desorption rate constant. The hydrogen desorption rate constant exhibits Arrhenius behaviour and is defined as

$$k_d = v_d \exp\left(\frac{-E_d}{k_b T}\right) \tag{1.3}$$

where k_b is the Boltzman constant, and v_d and E_d are functions of surface coverage [3].

Figure 1.2 shows a series of EFTIR thickness measurements taken during a run

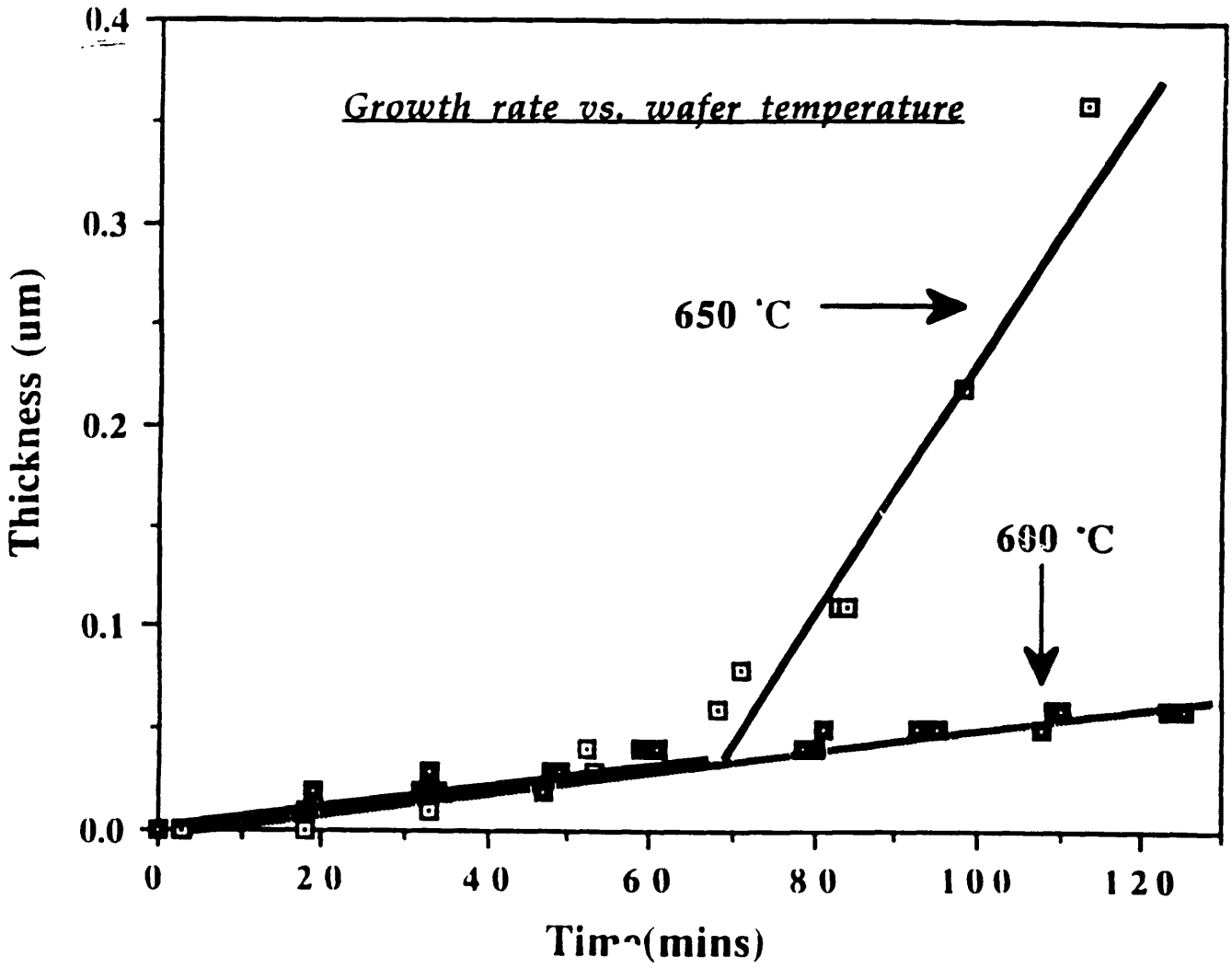

Figure 1-1: Measurements of epitaxial film thickness for two different temperatures.

using the UHV reactor [4]. The graph clearly indicates a linear growth rate at a constant temperature as suggested by the model.

1.3 Work Outline

The first stage of this thesis was to derive a comprehensive model of the process for the particular temperature regime of operation, based on experimental results and the theory of epitaxial silicon deposition. Next, the system was characterised in terms of its control variables to facilitate design of the controller. Finally, a controller was designed and implemented using several different control paradigms which were then compared.

A number of key issues were addressed in the design and implementation of the controller. To begin, there is a lack of continuous thickness measurements during the course of a run. A thickness measurement is generated only once every 40 seconds. Along with the time delay, there are also significant measurement and system noises associated with this wafer state measurement; quantization of the measurement is one such significant problem. The measurement of system variables such as temperature and pressure present similar problems of system and measurement noise. Additionally, there may be non-linearities associated with some of the system variable sensors.

The design of the controller focussed on the critical (according to the model), measurable wafer state and proces environment system variables. The approach to controlling these parameters was through the design and implementation of a multi-loop feedback system. For estimation of these parameters given system and sensor noise, techniques such as averaging and Kalman filtering were used. The final control archtecture consists of a fast inner loop to control process state parameters and a slower outer loop which uses thickness measurements to update the process model and implicitly the inner loop set-point.

This thesis is organised as follows. Chapter 2 develops the system model of the epitaxial process in terms of the measurable parameters. Chapter 3 presents the design and implementation of the inner-loop controller for our system. The performance of several controller designs are compared and the best one chosen for use in the epitaxial growth control system. Chapter 4 presents the overall outer-loop controller. Several different paradigms are considered and simulated and compararisons based on system performance are made. Chapter 5 is a summary of this thesis. A discussion of the work and proposed future work is presented.

Chapter 2

Epitaxial Growth Model

2.1 Introduction

In order to facilitate adaptive control of the epitaxial process being examined, a model which is able to describe the process given the operating conditions must be developed. These model parameters will then be updated continually during a process as the process moves from one region of operation to another. In this chapter, the epitaxial growth rate model for the operating conditions will be examined. To evaluate the values of the parameters of the model, experimental results from the reactor are fitted to the growth rate model and then compared to other published results. For the purposes of control, the sensitivity of the model with respect to controllable parameters will also be examined.

2.2 Model Development

Advances in the understanding of basic gas phase reactions for homogeneous silane pyrolysis have led to general models of silicon deposition kinetics. However, there is still a general lack of detailed models of the surface heterogeneous decomposition kinetics. For Very Low Pressure CVD (VLPCVD) of silicon and reduced temperatures, the homogeneous decomposition is suppressed and consequently, deposition uniformity improved.

The CVD process under consideration uses 100% silane. Greve and Racanell [2] characterizes this epitaxial deposition by a four stage chemical process [5].

$$2SiH_4 + 4^* \Longrightarrow 2H^* + 2SiH_3^* \tag{2.1}$$

$$2SiH_3 + 2^* \Longrightarrow 2H^* + 2SiH_2 \tag{2.2}$$

$$2SiH_2^* \Longrightarrow H_2 + 2SiH^* \tag{2.3}$$

$$2SiH^* \Longrightarrow 2^* + film + 2H \tag{2.4}$$

where * represents a surface site.

Equations (2.1) and (2.2) describe the adsorption of silane. These reactions have an Arrhenius rate constant k_{ads} and an activation energy E_{ads}. Equations (2.3) and (2.4) describe the incorporation of silicon onto the surface. This process can be described with a rate constant k_{inc} and an activation energy E_{inc}.

Assuming steady state and a sequential reaction, the growth rate, G, is given by

$$G = k_{ads} P_{SiH_4} (1 - \theta) N \tag{2.5}$$

where θ, the fractional surface coverage is defined as

$$\theta = \frac{k_{ads} P_{SiH_4}}{k_{inc} + k_{ads} P_{SiH_4}}. \tag{2.6}$$

Additionally, N is the total number of surface sites and P_{SiH_4} is the partial pressure of silane.

For this process there are two limiting conditions; the absorption limited case and the incorporation limited case. In the absorption limited case, the surface coverage θ is low ($\theta << 1$); consequently, the absorption site availability is high and hence the absorption is limited by the silane interaction with the surface. For this limit, (2.5) can be approximated by

$$G \approx k_{ads} P_{SiH_4} N. \tag{2.7}$$

As expected, this rate depends mainly on the adsorption rate constant and is also pressure dependent.

In the other limit where surface coverage is high ($\theta \approx 1$) the growth rate (2.5) reduces to

$$G \approx k_{inc} N. \tag{2.8}$$

In this limit, the growth kinetics depend on the incorporation rate constant only. The model does not have any pressure dependence, only temperature, by way of the Arrhenius rate constant k_{inc}. This is the limit of greatest interest since it corresponds to the regime of operation under consideration for VLPCVD. For this regime, with pressure less than 3 milliTorr and temperature less than 650°C, this model shows good model congruence with the measured results.

All operations, however, lie somewhere between these two limits and hence both reaction rates must be considered for an accurate growth rate model.

Reif and Comfort [5] present a detailed derivation of the above model and a discussion, based on experimental results, of the reaction kinetics of epitaxial silicon under different growth conditions.

2.3 Factors Affecting Model Parameters

There are several factors which affect the model and give rise to variation in model parameter values from wafer to wafer. The variation for the temperature/pressure regime of operation, can be attributed to wafer surface interactions. The presence of defects and particles on the wafer surface in general disrupts the growth process. In general, their net effect is to lower the available number of surface sites for incorporation (N) at the surface [5]. Considering the growth model, this would not affect the activation energy of the actual process.

Variation in growth rate between (100) and (111) oriented surfaces, where a (100) surface grows at a faster rate than a (111) surface are reported in [5]. Figure 2-1 shows the difference in growth rate between a cleaned surface and a surface which was not cleaned. Both of these effects can be incorporated into the model based controller.

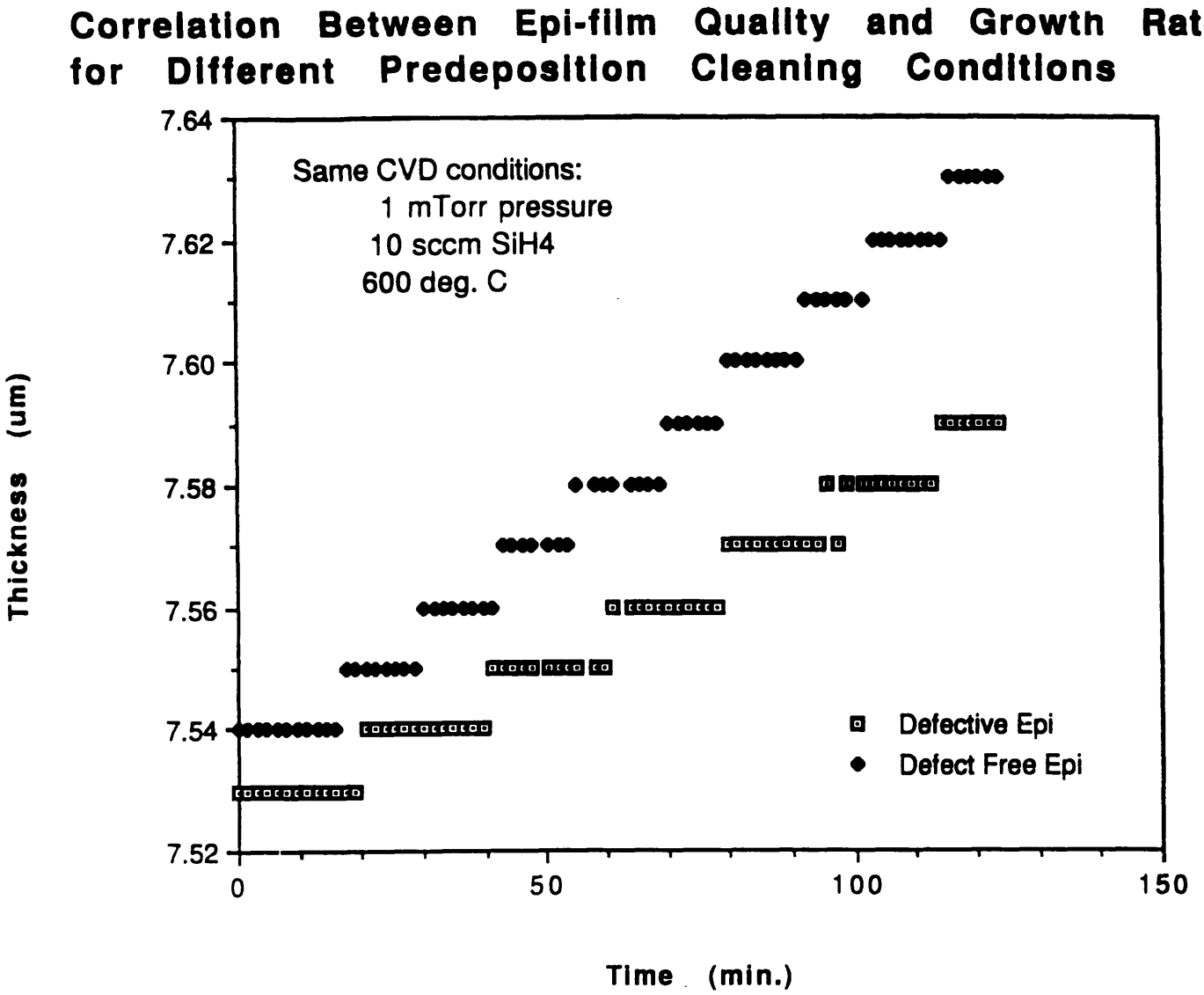

Figure 2-1: Epitaxial film growth under different initial cleaning conditions

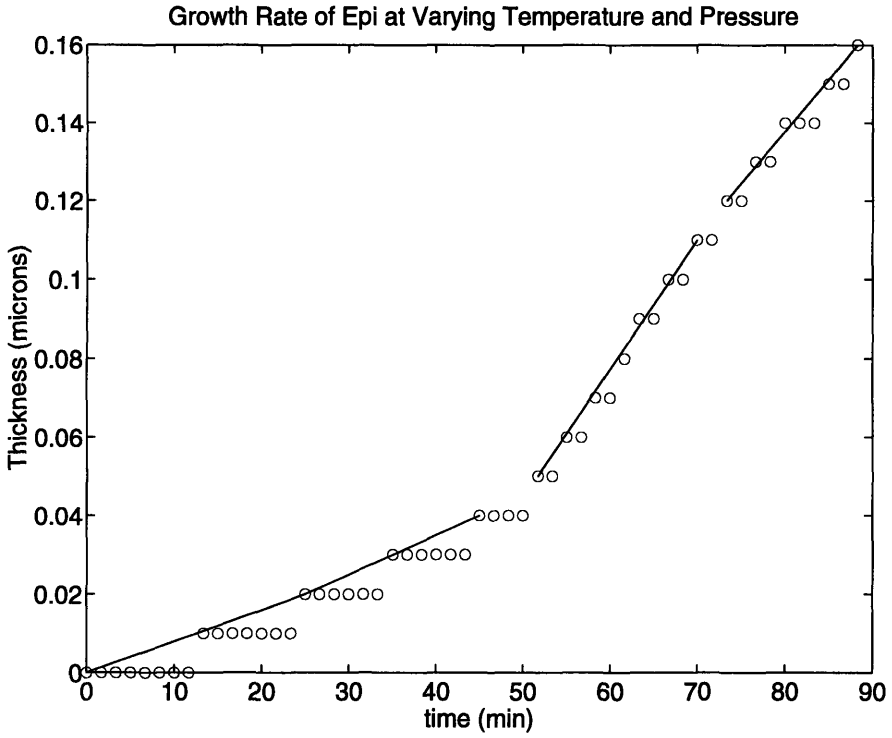

Figure 2-2: *In-situ* thickness measurements for various growth conditions.

2.4 Model Parameters

In order to evaluate the model parameters for the system, several runs were performed at different pressures and temperature. Using these results, the model parameters were solved simultaneously. Figure 2-2 shows *in-situ* thickness measurements taken from the reactor. The results exhibit the growth rate of the film for different temperatures and pressures. The temperature and pressure for these experiments were controlled by separate feedback controllers (the temperature controller is described in chapter 3). Table 2.1 is a summary of the results that were attained.

From Table 2.1 it can be deduced that the growth rate of the film is dependent on both the temperature and the pressure. However, it is much more sensitive to small changes in temperature as compared to pressure. A hundred percent increase in pressure at 600°C results only in an 18% increase in growth rate. Comparatively, increasing the temperature by 6% at 1 milliTorr increases the growth rate by 212%. This is the general result expected according to the model of VLPCVD silicon depo-

Growth Rate (microns/minute)	*Pressure (mTorr)*	*Temperature (°C)*
8.57×10^{-4}	1	600
1.5×10^{-3}	2	617
1×10^{-3}	2	600
3.27×10^{-3}	2	650
2.66×10^{-3}	1	650

Table 2.1: Growth rate measurements for various growth conditions.

sition for this temperature/pressure regimes. The results show, as expected, that for temperatures below 650°C the growth model can be approximated to the high surface coverage limit which is independent of the pressure of operation. However, even at 650°C the effects of pressure variation are significant enough for the general model to be used in evaluation of the growth rate for those parameters.

To evaluate the model parameters ($K_{ads}, K_{inc}, E_{ads}, E_{inc}$), a two step approach was taken. The first step was to solve for K_{inc} and E_{inc} assuming the high surface coverage regime for measurements taken at 2 milliTorr, 600°C and 2milliTorr, 617°C. Hence

$$G = NK_{inc_0}e^{\frac{E_{inc}}{RT}}. \tag{2.9}$$

Solving simultaneously,we find $K_{inc_0} = 2.549 \times 10^{-7}, E_{inc} = 37Kcal/mole$. These results are comparable with results reported and compared with other sources in [5]. Comfort and Reif [5] expects the overall activation energy of the reaction (E_a) for this regime to be $\approx$ 40Kcal/mole. Sinniah [3] reports it to be 47Kcal/mole.

Using these results, a least square curve fit was done by minimizing the deviation of the model from the measured results. For this optimization, we used the general formula where

$$G = \frac{P_{SiH_4}NK_{ads_0}e^{-\frac{E_{ads}}{RT}}}{1 + P_{SiH_4}\frac{K_{ads}}{K_{inc}}e^{-(\frac{E_{ads}-E_{inc}}{RT})}}. \tag{2.10}$$

The results from this optimization give us the results

$$K_{inc_0} = 11.3501 \times 10^{-5}, E_{inc} = 52Kcal/mole \tag{2.11}$$

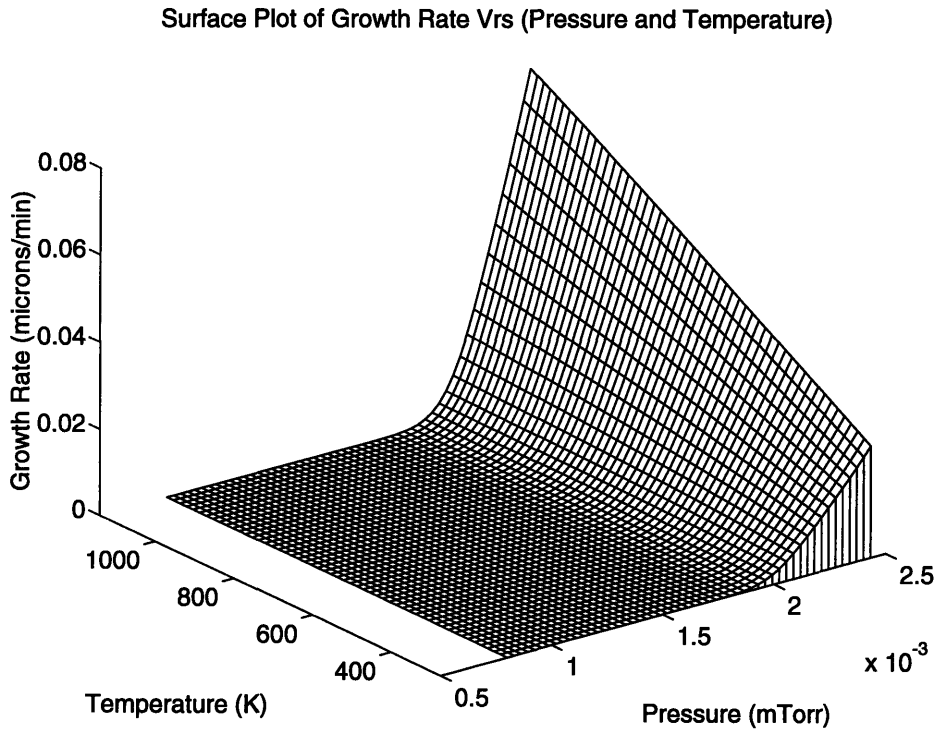

Figure 2-3: Growth rate of model with changing temperature and pressure.

$$K_{ads} = 9.5973 \times 10^{-12}, E_{ads} = 12.2 Kcal/mole. \tag{2.12}$$

Figure 2-3 shows a three dimensional plot of growth rate as the pressure and temperature vary using the model described and the constants derived above.

It is important to note that for the control approach, these values are only important for the initial startup of the process. During the process run, measurement information will be used to update one or more of these parameters. It is essential, however, that the model form is accurate.

2.5 Sensitivity

For control purposes, it is necessary to analyse the model sensitivity to changes in parameter values. Specifically, in this case, the model's sensitivity to changes in pressure and temperature – the parameters to be controlled – is examined.

Taking the derivative of (2.10) with respect to temperature (T)

$$\frac{\partial G}{\partial T} = \frac{-\frac{b}{T^2}Pae^{-\frac{d}{T}}(1+Pce^{-\frac{b}{T}}) - P^2ac\frac{d}{T^2}e^{-\frac{(b+d)}{T}}}{(1+Pce^{-\frac{d}{T}})^2} \tag{2.13}$$

and the derivative of (2.10) with respect to pressure (P)

$$\frac{\partial G}{\partial P} = \frac{ae^{-\frac{b}{T}}(1+Pce^{-\frac{b}{T}}) - Pace^{-\frac{b+d}{T}}}{(1+Pce^{-\frac{d}{T}})^2} \tag{2.14}$$

where

$$a = N * K_{ads}, b = E_{ads}, c = \frac{K_{ads}}{K_{inc}}, d = E_{ads} - E_{inc}. \tag{2.15}$$

2.6 Control

The model developed in this chapter forms the basis for the hierarchical control structure developed in chapter 3 and 4. In our controller, the model determines the parameter set-points for operation. Additionally, the model is periodically adapted as new measurements are collected.

Chapter 3

Design and Implementation of the Temperature Loop Controller

3.1 Introduction

The critical control loop in the overall system is the temperature controller. Theoretical models of silicon epitaxy growth indicate that for low temperature, low pressure conditions, the growth rate of the process is strongly dependent on the surface temperature of the wafer. Experimental data taken from the epi-reactor used in our experiments and in [4] show, as predicted, that the temperature of the wafer is the critical factor influencing the growth rate of the silicon.

As described above, the approach for controlling the epitaxial film growth rate is to control the temperature of the wafer, maintaining the temperature at a prescribed level given the growth rate required. To design and implement such a controller, a system model of the reactor was first realized. This model describes the temperature dynamics of the reactor with respect to its control inputs. The model forms the basis for the eventual design of the controller and must incorporate all the necessary temperature characteristics of the reactor. Using this model, several controllers for the system were designed and evaluated. The final controller was then selected and the performance of the final system compared to the un-compensated system. The main objective of the controller design was to achieve good temperature stability and

controllability of the wafer on which the silicon was being deposited.

3.2 Reactor and Control System

Figure 3-1 [1] shows a schematic of the epitaxial reactor. Mounted inside the CVD chamber, where the wafer sits during operation, is a resistive and radiant heater. This graphite heating filament is coated with silicon-carbide and has a temperature range up to 1000°C. To minimize heat loss to the sides of the CVD chamber, there are heat shields surrounding the filament.

Figure 3-1: The LPCVD epitaxial reactor schematic.

3.2.1 Heating System

The electrical power which is needed by the filament to heat up the chamber is met by an electrical power supply [6]. For our work the power supply used was the Sorensen DCR-150-18B. This power supply was externally controllable current and voltage output levels, and is directly connected to the filament. The power supply has the capacity to output a voltage from 0 to 10V and a current range of 0 to 20 Amps.

For our work, the power supply was configured to be voltage controlled and current limited. Hence, the temperature desired for the particular run corresponded to a particular control voltage level output. To protect the power supply, both the output voltage and current were limited. The voltage was limited to 2.7V. This voltage level corresponds to the maximum current limit, 18A – protecting the power supply from overloading.

Figure 3-2 shows the wiring schematic for control of the power supply. The input to this circuit is supplied by the control computer, a MacIntosh Quadro using an interface card with Digital-to-Analog (D/A) converters, in our case the Lab NB card produced by National Instruments. The D/A under command of LabView 2.2 software (also from National Instruments) sources ± 1 Amp as required by the power supply control circuitry. The card was configured to supply a variable voltage with a range of 0 to 5 V.

3.2.2 Temperature Sensing

In order to control the wafer temperature by varying the input voltage to the heat filament, the actual temperature of the wafer must be measured in real time and compared to the desired temperature. For the system, there are two methods of sampling the real time temperature of the wafer.

Behind the wafer chasm is mounted a thermo-couple. The thermo-couple supplies a voltage which is proportional to the temperature of the chasm. The second method used to measure wafer temperature is via an optical sensor. Through a glass window in the chamber, the sensor uses infra-red radiation to measure the wafer tem-

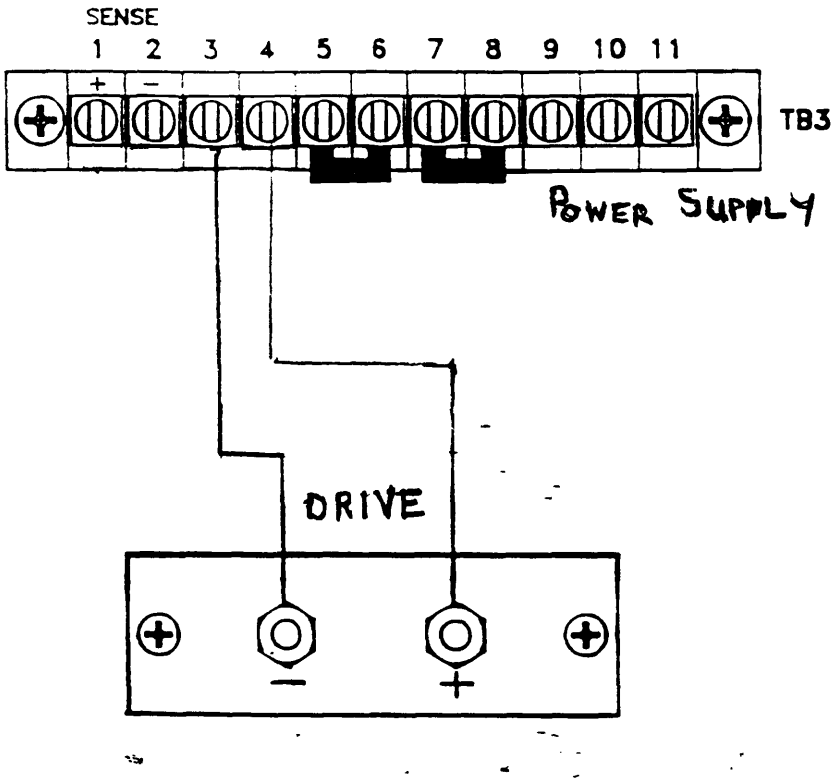

Figure 3-2: Wiring schematic of heater power supply.

perature, converting the temperature value to a proportional voltage output level. The voltage levels produced by the two temperature sensors are sampled using two Analog-to-Digital converters on the NB-MIO-16 interface card installed in the Mac-Intosh Quadro.

Figures 3-3 and 3-4 show a graph of sampled values from the thermo-couple sensor and the optical sensor respectively. The two graphs reading samples taken from the two sensors while the chamber/wafer temperature is held at a fixed temperature level. The thermo-couple sensor measurements contain a high amount of noise. Further analysis of the noise indicates that the noise is uniformly distributed around a mean value. A possible source of the noise is the electrical noise around and near the temperature sensor and the wires carrying the signal. This noise appears amplified in

our measurements because of the low signal levels which the thermo-couple produces. Other contributors to the observed noise are probably measurement noise associated with the thermo-couple and system noise.

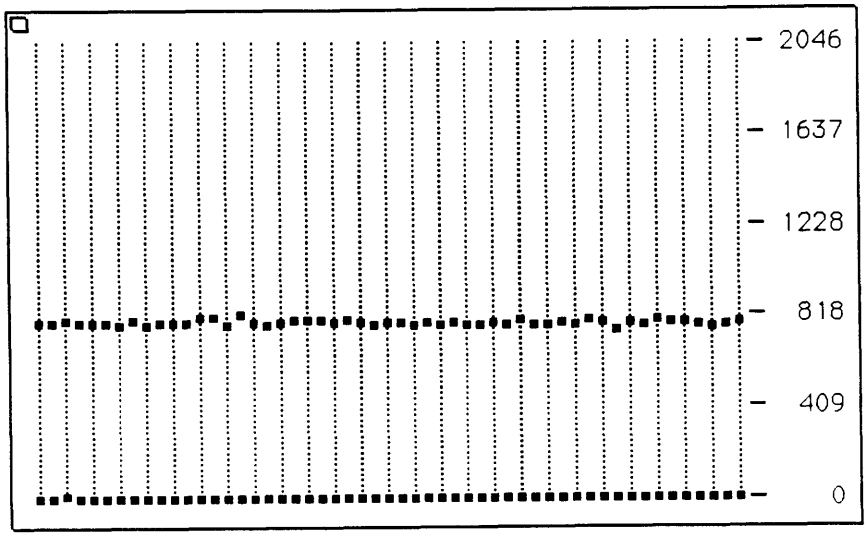

Figure 3-3: Optical sensor measurements for a constant wafer temperature.

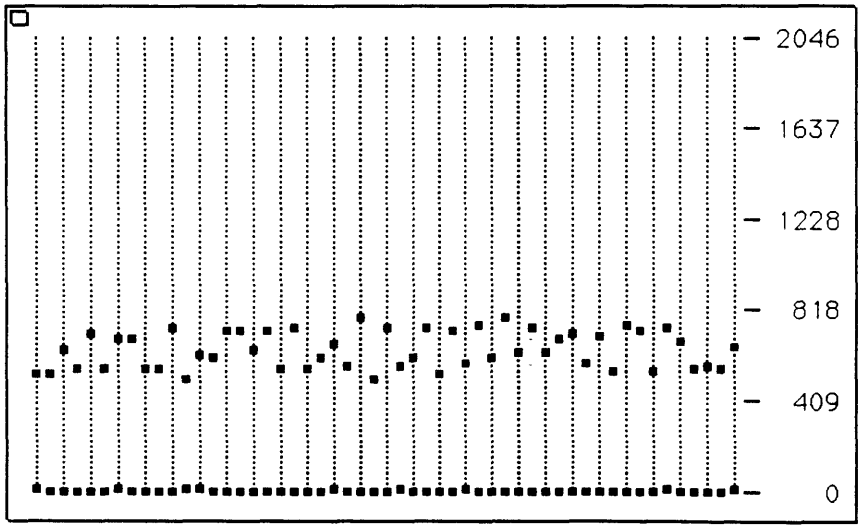

Figure 3-4: Thermo-couple measurements for a constant wafer temperature.

The noise associated with the optical sensor is very small compared to that of the thermo-couple. The measurements were normally distributed around a mean value.

This proportionally small noise is best attributed to measurement noise. Using a Kalman filter most of the noise is filtered from the signal; Appendix A describes the development of the Kalman filter used in our system. The main problem with the optical sensor is that of predictability from run to run. Any disturbance which affects the transmission of the optical rays to the sensor impairs the measurement. Hence, reflections and the presence of ionized gases in the chamber affect the relative temperature reading. Since these problems manifest generally as a constant offset, they cause only start up problems when using a feedback controller based upon the thickness measurements - as in this case.

3.2.3 Temperature Model

To determine a model to describe the dynamic temperature characteristics of the system, a number of experiments were performed. The resulting model compactly describes the system in terms of the pole and zero locations. For these experiments only measurements from the optical sensor were used.

The first experiment sought to determine the exact relationship between the input voltage to the heating filament and the eventual steady state temperature. Figure 3-5 is a plot of the results obtained. It shows that for the region of operation in which deposition will take place, there is a linear relationship between the input voltage and the output temperature.

The second experiment determined the open loop transient characteristics of the system by examining its response to step changes in input voltage. Figure 3-6 shows the temperature response to a typical step voltage increase (1.8V to 2.2V) and the response to the corresponding step decrease. As the graph shows, the dominant temperature time-constant for the system (cooling and heating) is approximately 87 seconds.

Together the steady state and dynamic characteristics indicate that our system behaves as a first order linear system, allowing us to implement a linear feedback controller for temperature regulation.

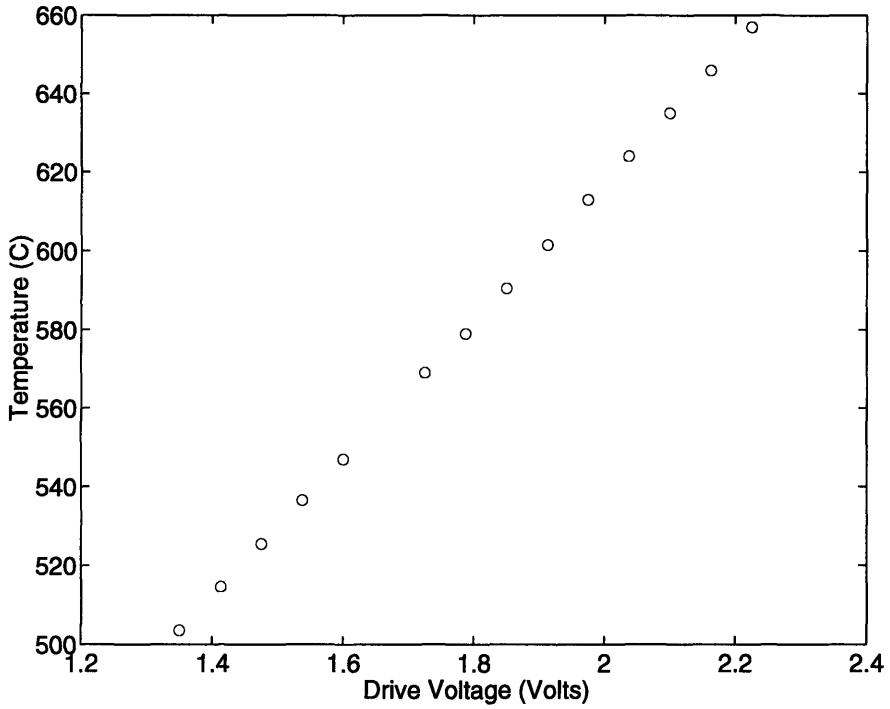

Figure 3-5: Heater drive voltage versus steady state system temperature.

3.3 Controller Design

There are several objectives in the design of the temperature controller. The first objective is to reduce the overall time constant of the system from 87 seconds to an acceptable value to ensure that the overall system will be quick acting. The second objective is to protect the power supply by minimising fluctuations and maintaining an upper and lower limit on its control input. Finally, we seek to ensure that the overall system is robust with good high frequency noise rejection.

The final design selected for the negative feedback system was the best compromise of the above mentioned objectives.

From the experiments described above, the system was modeled in the frequency domain with an open loop pole located at 87 seconds and a gain of 857. Figure 3-7 shows a Bode plot of this system. Since the system to be implemented is digital, this is a Bode plot of the sampled model of the system. In this plot we assume a sampling frequency of 2×10^{-4} seconds.

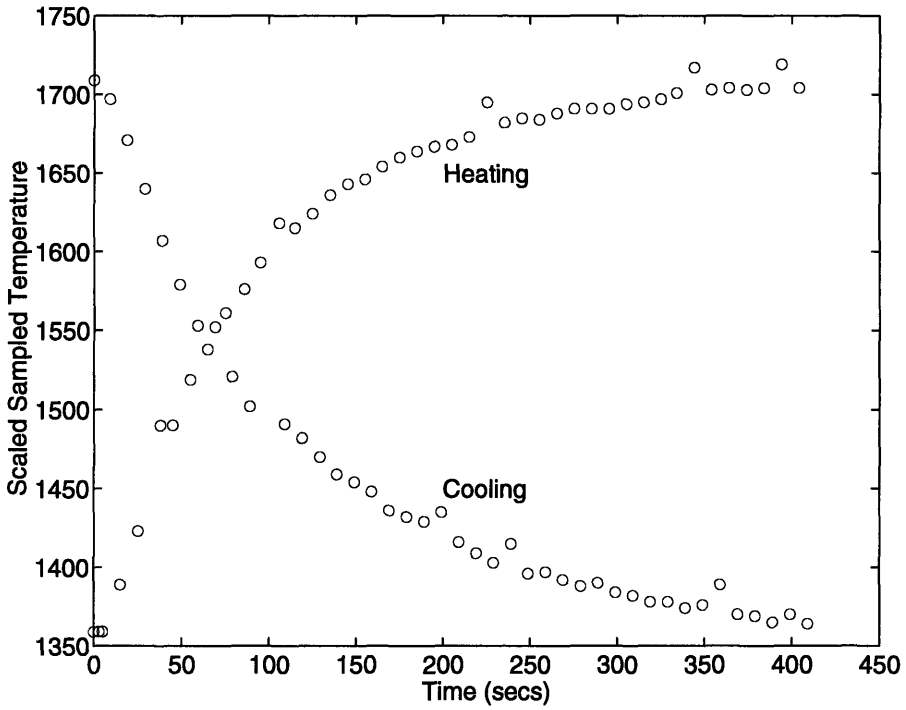

Figure 3-6: Heating and cooling time constants; response to a step voltage change is shown.

To achieve our design objectives, large open loop low frequency gain, high cross-over frequency and good phase and gain margins were needed. The high low frequency gain was needed to limit the steady state error of the system. The high cross over frequency is needed for quick system reaction while the gain and phase margin ensure stability of the system.

The effects of sampling and time delays inherent in the system contribute increasing negative phase at high frequencies. These effects limit the maximum cross over frequency for stable operation.

3.3.1 Compensator Design

For the feedback loop in the temperature controller, three types of compensators were examined. Three digital compensators were simulated and implemented. After comparing their performances in terms of noise rejection, speed and least fluctuation in input voltage to system, one of the compensators was selected. Three compensators

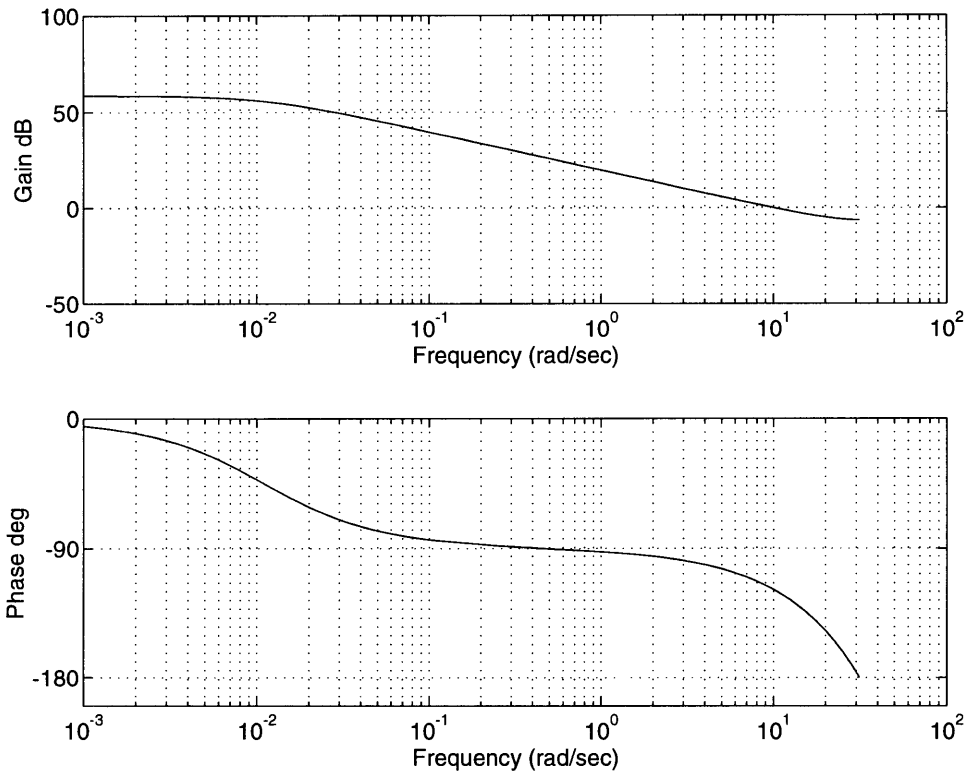

Figure 3-7: Sampled Bode Plot of System

were examined: a simple gain, a pole zero (PZ) and a PID. In each case an interactive method was used to implement a best solution given our objectives described above.

In the case of the simple gain approach the overall system exhibits good low frequency gain and high frequency cross over. However, it also exhibits poor high frequency noise filtering. Figure 3-8 shows a Bode plot of the open loop system with a simple gain compensator. This Bode plot, as all the other compensated systems, assumes a sampling time of 2×10^{-4} seconds.

To enable better cross-over frequency characteristics, a low-frequency zero and a higher frequency pole were used as the compensator. Figure 3-9 shows a Bode plot of the overall system using this filter. For this system, the system function for the compensator was

$$\frac{k(z+0.5)}{z+.9} \tag{3.1}$$

The effect of the additional higher frequency pole was to allow for higher low fre-

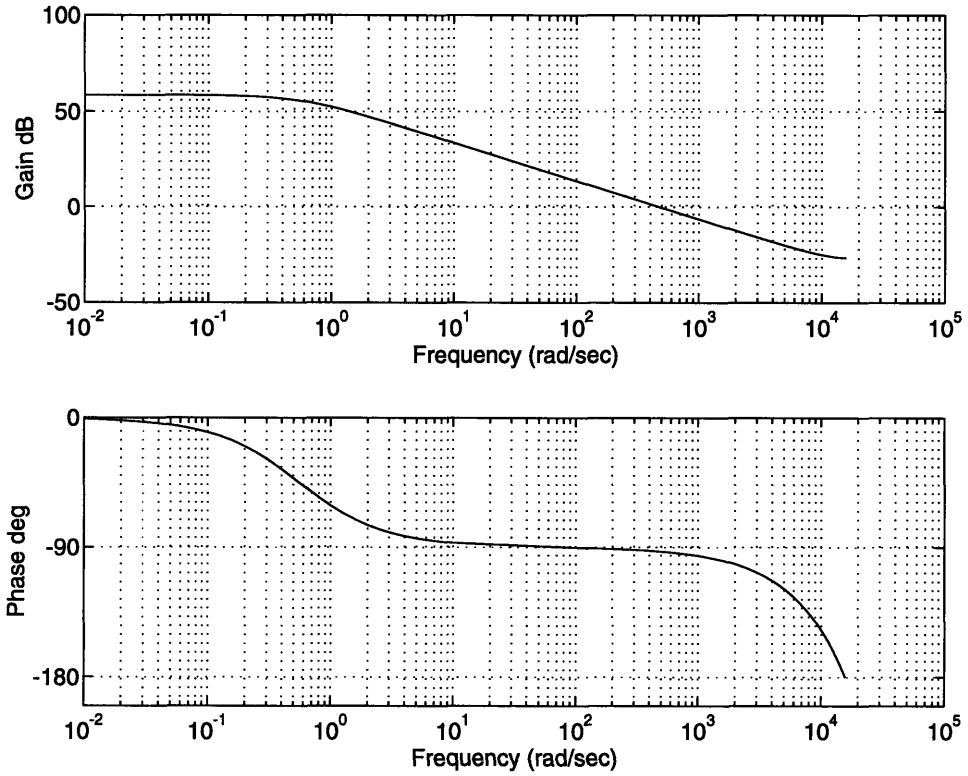

Figure 3-8: Bode plot of open loop simple gain compensated system.

quency gain with the limitation of good phase margin at crossover; this was accounted for by the appropriate gain and zero location. As indicated above, however, one of our objectives was to ensure that the system was not overly responsive - to minimize the fluctuations of the drive signal. Hence, for our practical implementation, the cross over frequency was reduced interactively to an acceptable value by manipulation of the gain and zero location.

For better reset characteristics (to minimize steady-state errors), a pole is added at zero completing a PID system which encompasses the above described characteristics of the other systems. An appropriate gain was selected to minimize the output sensitivity. Figure 3-10 shows the Bode plot of the open loop system compensated with this system.

$$\frac{k(z+.5)}{z(z+.9)} \tag{3.2}$$

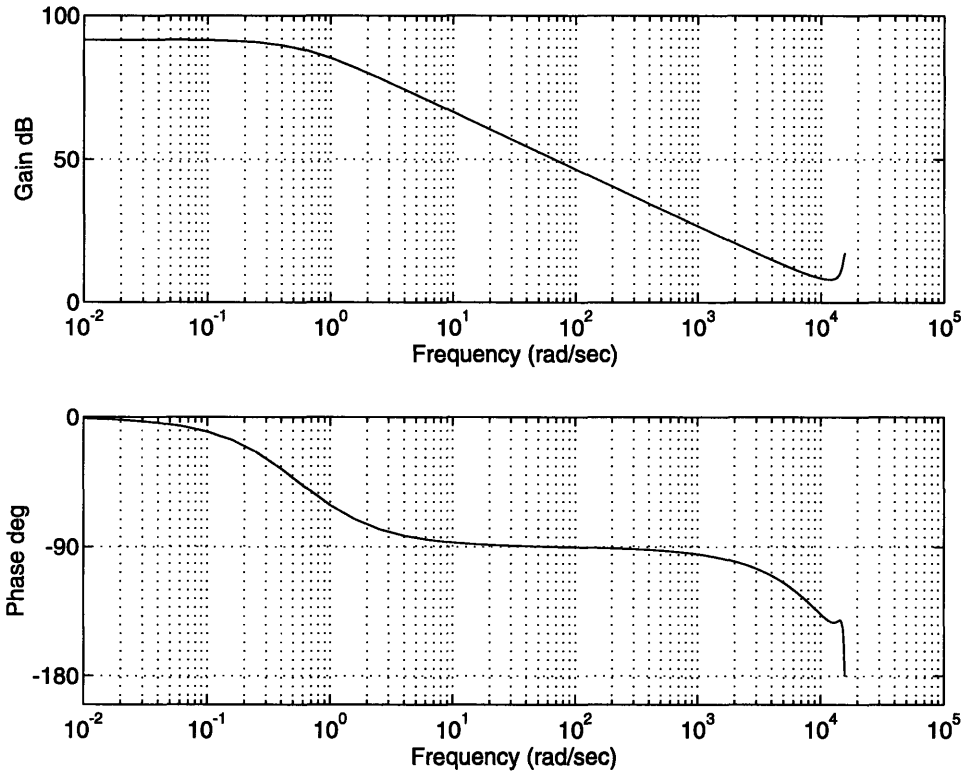

Figure 3-9: Bode plot of open loop pole-zero compensated system.

3.4 Practical Issues

To implement the controllers using our hardware and software platforms, there were several practical issues that were addressed. One of the most important issue was that of *in-situ* cleaning.

Before each run begins, a UV cleansing procedure must be performed in the chamber. During this procedure (approximately 5 minutes at the deposition temperature), the optical sensor cannot be used since its measurements will be greatly affected by the presence of the UV radiation. Our practical solution is to simply shut off the temperature control loop during the cleaning process and to use the set point before the clean as the drive input. This procedure is reasonable since the temperature drift during the short 5 minute period is not expected to be significant.

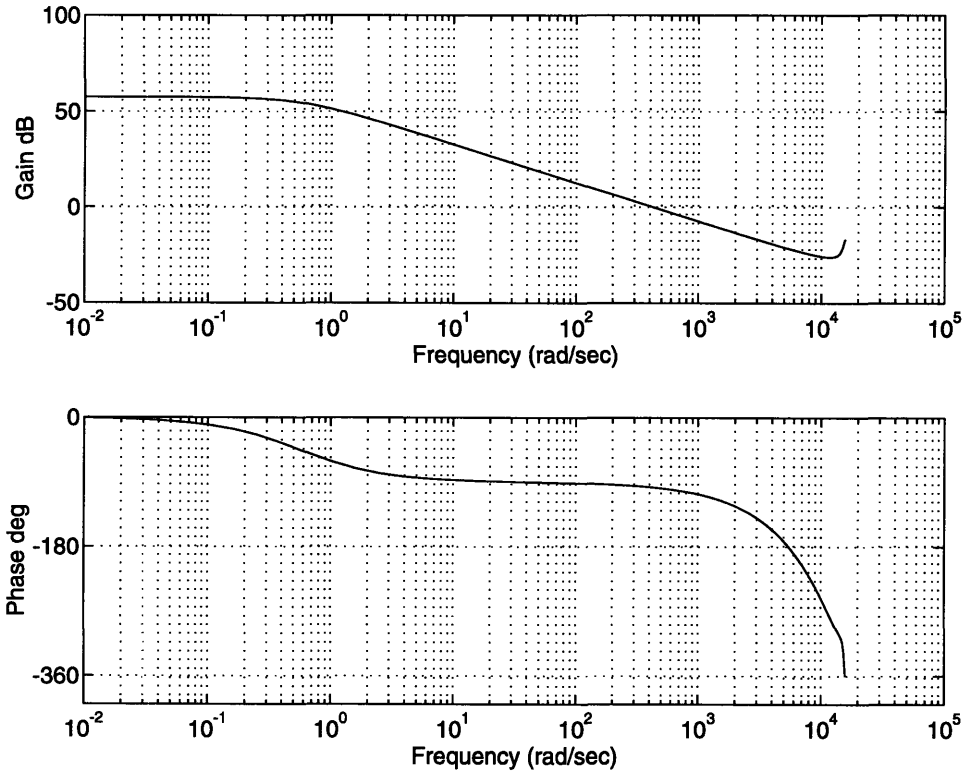

Figure 3-10: Bode plot of open loop PID compensated system.

3.5 Results

The following presents measurements taken of the temperature and drive voltage during step changes in desired temperature while the system was under temperature control. For each compensator, the temperature is allowed to settle at 1700 units. This output from the A/D is a linearly scaled value of the actual temperature. For the system, the sampled value, $S_T = T \times a + b$, with $a = 9.09$, and $b = -3173$. The desired temperature was then changed from 1700 units (corresponding to 536.5^o C), to 2200 units (corresponding to 590.5^o C). Figure 3-11, Figure 3-12 and Figure 3-13 show the results of these experiments under simple gain, PZ and PID compensator control respectively.

Evaluating the performance of the three compensators by comparing their performance in the time domain, it is clear why the simple gain compensator was not selected. The fluctuations of the drive voltage (min $\approx 0V$) was very high compared to those of the PZ and the PID controller. The drive voltage performance for the

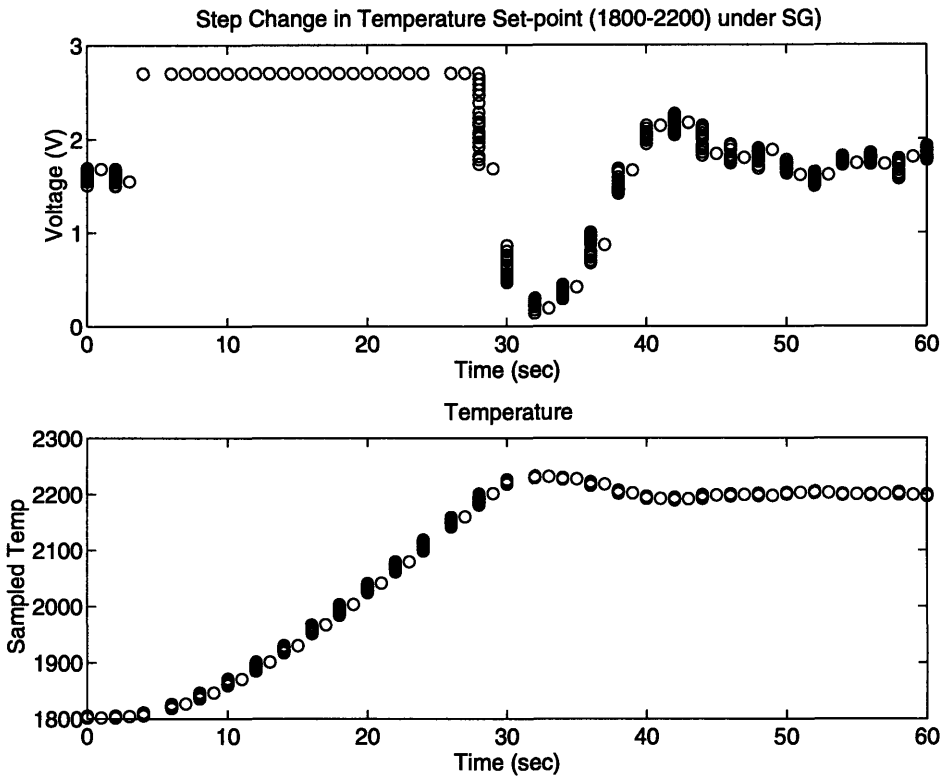

Figure 3-11: Temperature and voltage measurements during step change in desired temperature set-point under simple gain compensation.

PID and PZ are comparable with respect to their value fluctuation. However the PID compensator was selected because of its steady state error behaviour not easily shown from the above graphs.

Figure 3-14 shows thickness measurements during a run using the PID controller in our feedback temperature inner loop. Growth was performed at 1 milliTorr and 600°C for the first 50 minutes. A step change in desired temperature is made after 50 minutes to 648°C. The graph shows the constant growth rate expected during periods of constant temperature.

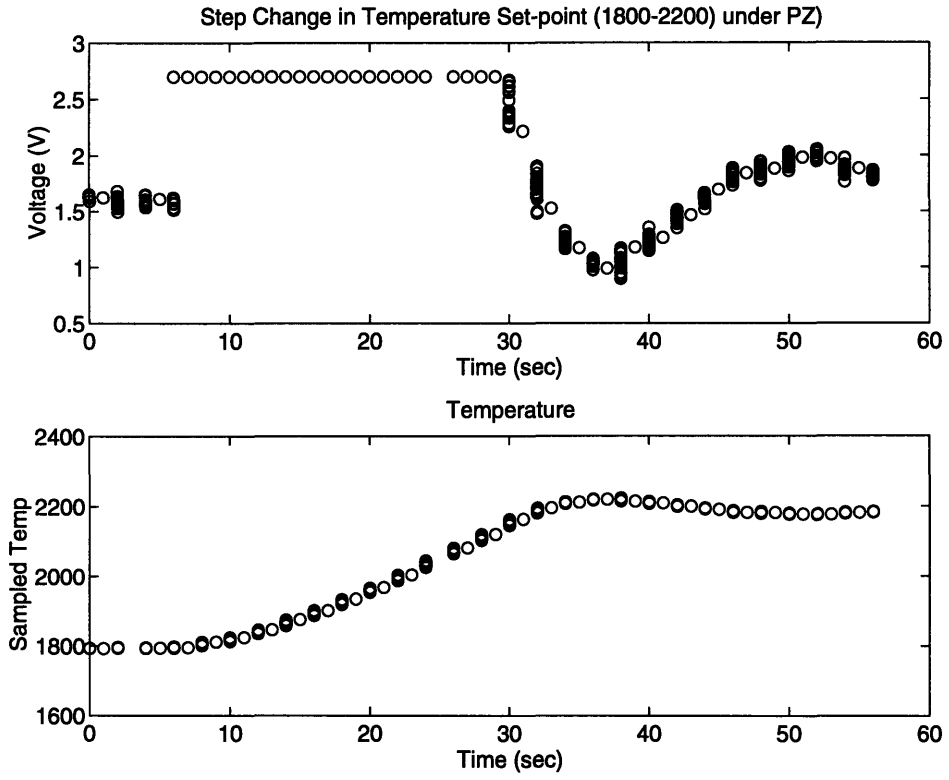

Figure 3-12: Temperature and voltage measurements during step change in desired temperature set-point under PZ compensation.

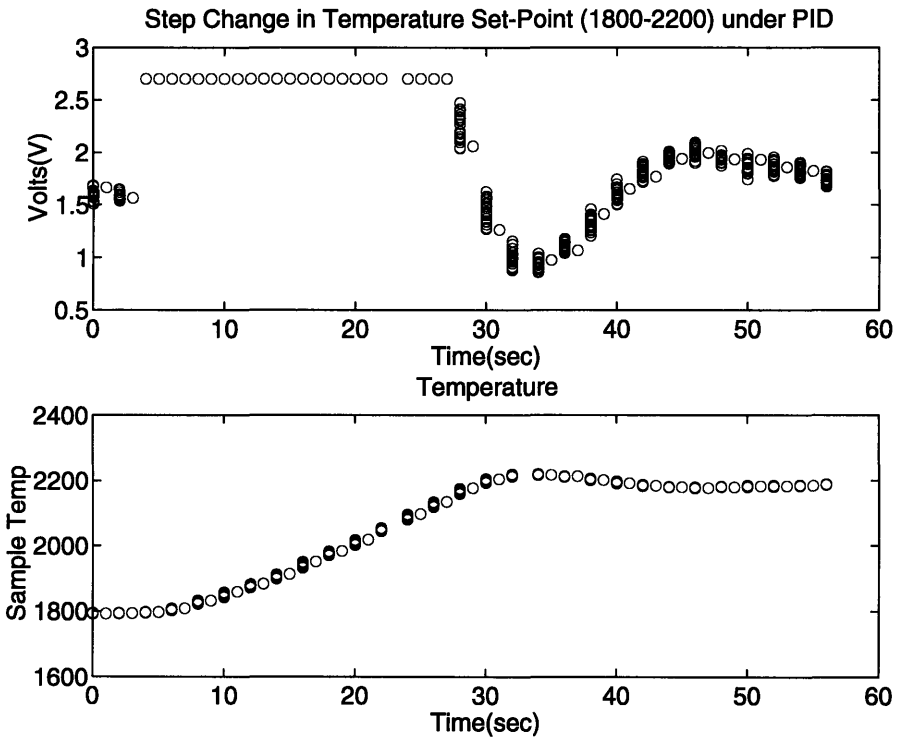

Figure 3-13: Temperature and voltage measurements during step change in desired temperature set-point under PID compensation.

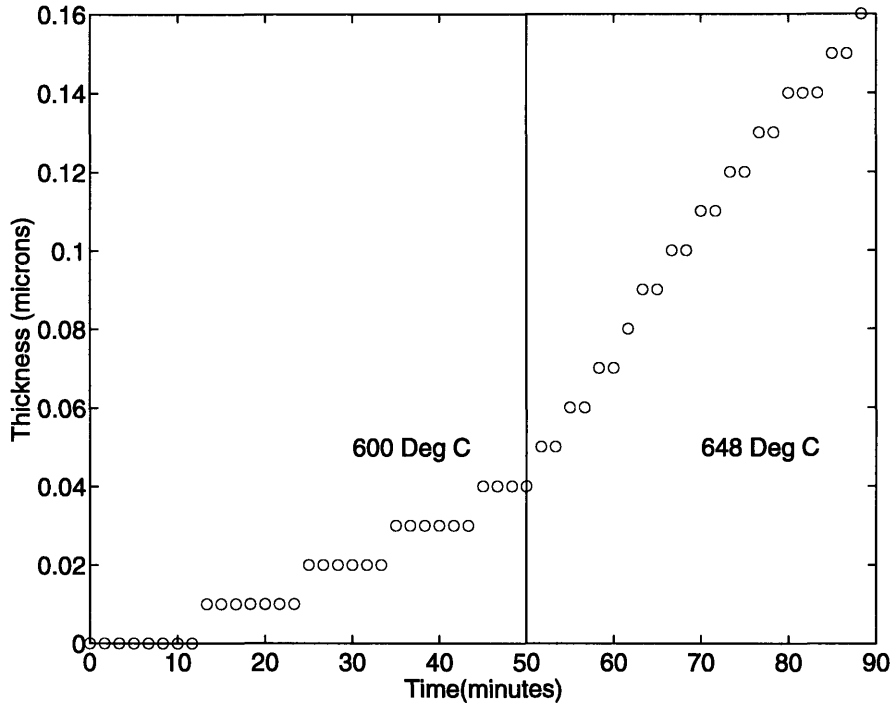

Figure 3-14: EFTIR thickness measurements under PID controlled temperature.

Chapter 4

Design and Implementation of the Outer Loop Controller

4.1 Introduction

Our hierarchical control system is completed by the outer loop controller which, as described above, essentially supplies control commands to the inner control loop. In this sense, the role of the outer loop is to account for the inaccuracy of the inner loop in attaining our desired growth rate. This inaccuracy stems from the changes in model parameters, reactor conditions and un-modeled behaviour of the system. The outer loop accounts for these differences between the desired growth rate and the actual growth rate by effectively changing the parameter set-points of the inner control loops based upon our model. Additionally, the outer-loop effects the recipe instruction sequence during a run.

In this chapter, we will examine the performance of several outer-loop controllers. First, the control paradigms for the different controllers will be discussed, in the process analysing their design procedures, inherent limitations and advantages. Secondly, the simulated behaviour of our system is outlined. These simulations serve to anticipate the behaviour of the actual system after implementation. Finally, a description of the actual implementation is presented together with the actual performance and behaviour of our system. Here, we present the hardware and software interface which

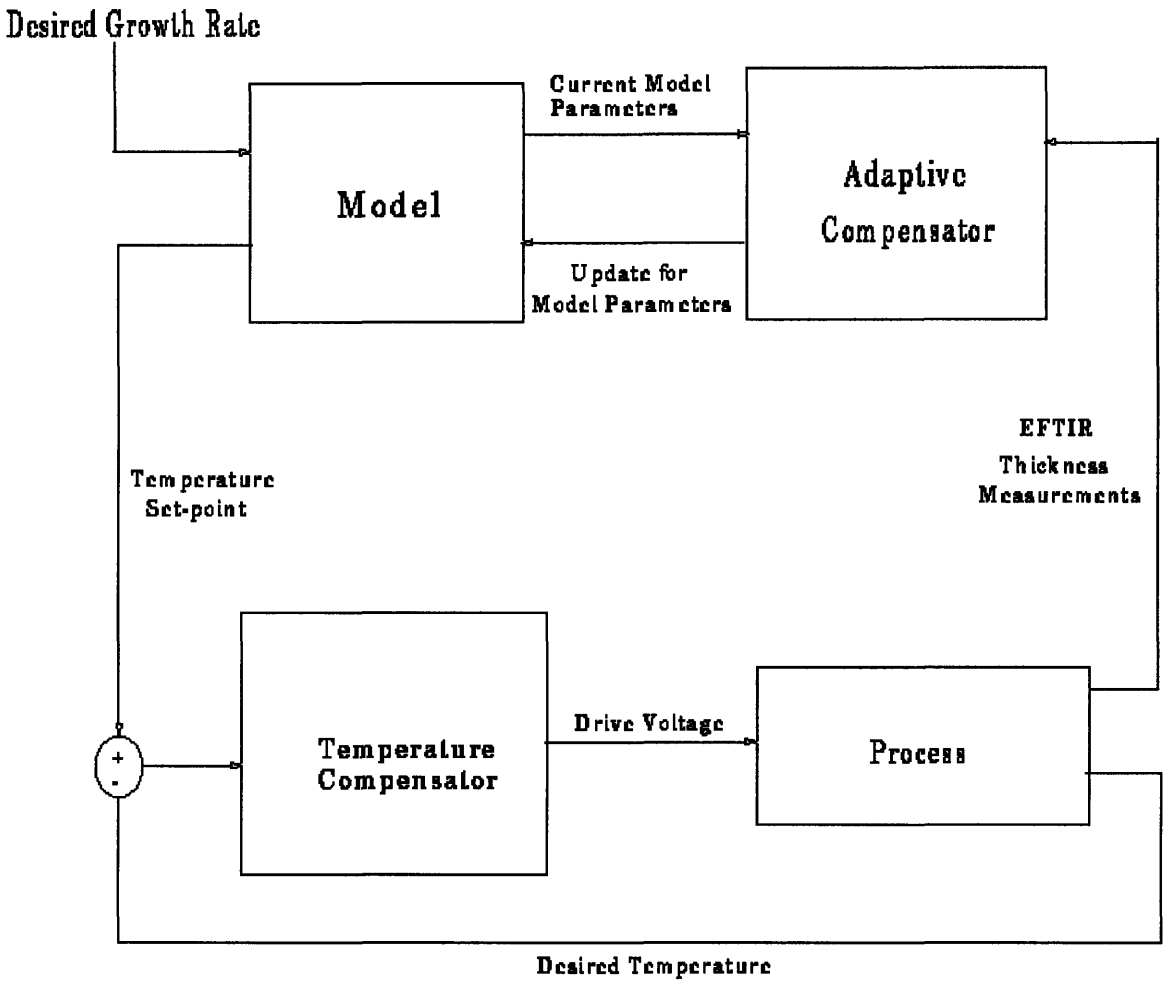

Figure 4-1: The hierarchical controller flowchart.

facilitated the controllers. We analyse the controllers in terms of their congruence with simulated behaviour and their ability to hit the target growth rate.

4.2 Controller Design

Figure 4-1 is a flow chart of the general structure for the implementation of an outer loop. As the figure shows, the outer-loop consists of our derived model of the system and a compensator. The reactor recipe, which consists of the desired growth rate, temperature and pressure for a particular run is supplied to our epitaxial growth model. The model is used to determine the temperature set-point required for the desired growth rate. This set-point is converted to a corresponding drive voltage value

(based on the temperature analysis of the reactor) and is fed to the power supply driving the heating element in the reactor. This is the input to the temperature loop, controlled as described above, by a feed-back loop using a digital PID compensator.

The outer-loop's inputs are the EFTIR thickness measurements which are converted to a growth rate value. Based upon these measurements, the outer-loop adjusts the parameter and/or model coefficients to account for the discrepancy between the expected growth rate and the actual growth rate. These new set-points are fed back to the inner-loop.

There were three main control structures that were analysed and implemented for our system. The first method simply assumes that our model of the system is correct, and hence, it only adjusts the temperature set point based upon a linearised model of the system. The second model assumes that the pre-exponential coefficient of our model changes from time to time based upon the wafer surface conditions, accounting for discrepancies. Hence this method adjusts the pre-exponential coefficient of our model and the temperature set-point implicitly. The third model is an extension of the second; it adjust the pre-exponential constant and the activation energy of our model based upon our latest data and the previous set of thickness measurements.

Our model for all three structures is the simpler Arrhenius growth model stemming from an assumption that our regime of operation is the low temperature/pressure region:

$$G = NK_{inc_0}e^{\frac{-E_{inc}}{RT}}. \tag{4.1}$$

This assumption is made for several reasons. Firstly for simplicity and ease of implementation; computations using the extensive model developed in chapter 2 are time consuming and difficult to implement. Secondly, given that our system is not expected to deviate significantly from the operating point, for the range of operation, our model approximation is a very good description of the system. Assuming that small changes in the growth rate at the operating point can largely be attributed to the changes in the parameters associated with the incorporation factor K_{inc}, the

simpler model is adequate for control.

4.3 Controllers

The following is a detailed discussion of the three other loop controllers examined.

4.3.1 Linearised Model Update

Using a linearised model update approach for the outer-loop controller, the parameters for the model are never updated or changed during the run. They are assumed to remain constant during the run. Hence, the implicit assumption is made that the point of operation is somewhere along the model curve. The objective of the controller is therefore to move the point of operation to that point by simply adjusting the temperature to the desired growth rate point on the curve.

In practice, this is accomplished by linearising the model curve at the initial point of operation and calculating the corresponding change in temperature which would correspond to the discrepancy between the expected growth rate and the actual growth rate. Figure 4-2 shows how the change in temperature is derived. This change in temperature, ΔT, is simply added (or subtracted) from the previous set point.

$$\Delta T = \frac{\partial T}{\partial G} \Delta G \tag{4.2}$$

and from (4.1)

$$\Delta T = \frac{RT^2}{NK_{inc_0} E_A \times e^{\frac{-E_A}{RT}}} \Delta G \tag{4.3}$$

where the new temperature set-point will now be $T_{old} + \Delta T$.

There are two forms of update which were analysed for this paradigm. In the first case, Type 0, T_{old} is always the initial temperature set by the model, therefore it does not change from measurement to measurement. This method is clearly limited, as will be seen from the simulations, because it assumes that the nominal point of operation is at the expected value, calculating the gradient curve at that point. This system is clearly not very effective for systems with drift or constant deviation from optimum.

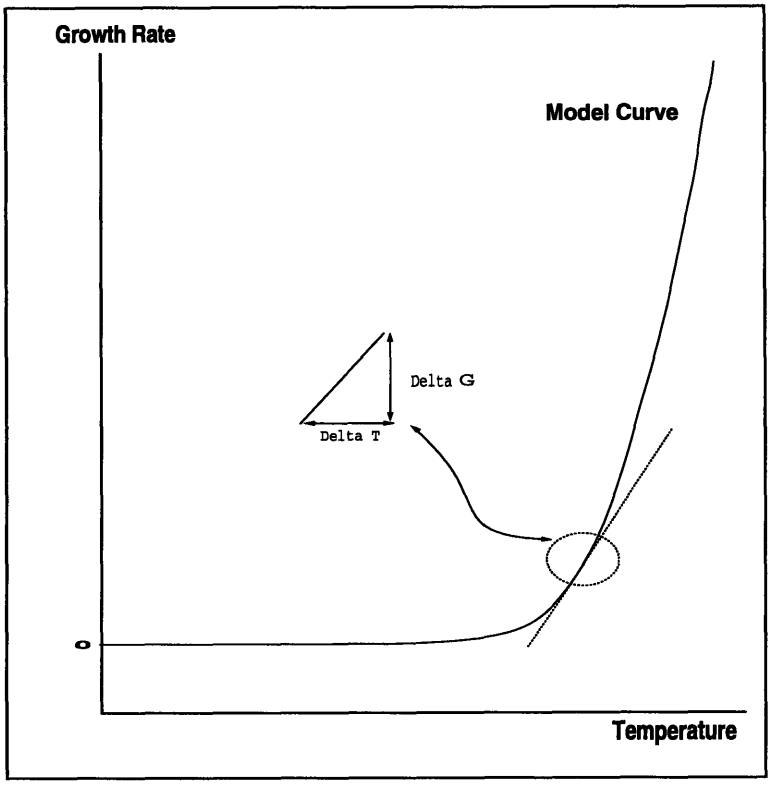

Figure 4-2: Linear outer loop control procedure.

In the second update method, Type I, the ΔT is calculated using the actual current temperature each time. The simulations below show a comparison between the two methods under expected system conditions.

The two linearised model methods provide a good reference point for evaluating our adaptive control structures.

4.3.2 Adaptive Controller - Pre-exponential

This approach assumes that the deviation of the model from measured results is due to changes in wafer surface or other system conditions that can be modeled by a corresponding value of the pre-exponential parameter. To effect this approach, we perform a simple model curve fit of the present measurement and the previous one. Both points are given equal weighting with past measurement values not used because of the relatively slow rate of thickness data acquisition.

Figure 4-3 shows graphically the adaptation procedure after a thickness measure-

ment. A new thickness measurement is used to calculate a growth rate corresponding to the temperature set-point between the two measurement. This value corresponds to the G_M in the figure. Using this value and (4.1), a new K_{inc_0} is derived – corresponding to a new model curve, as shown in the figure. Based upon this new model, a new temperature value which will correspond to the desired growth rate is derived and used as the new temperature set-point.

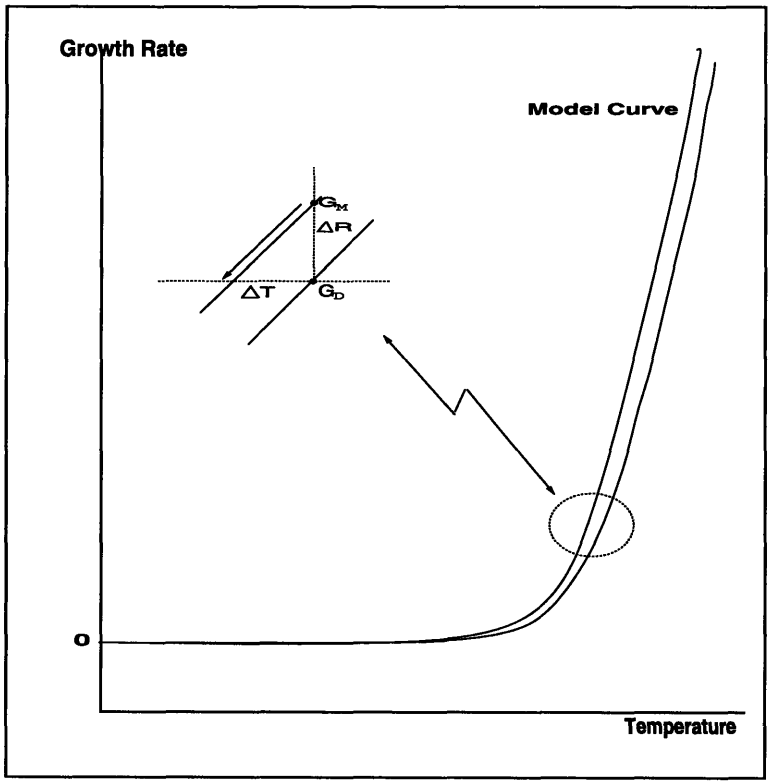

Figure 4-3: Adaptive procedure for pre-exponential constant based control.

After each measurement this procedure is repeated, thereby continually adapting the model. ΔT is the change in temperature set-point required for the desired change in growth rate, ΔG, using the model.

4.3.3 Adaptive Controller - Pre-exponential and Activation Energy

This approach for adaptive control of the outside loop extends the previous case by updating both the pre-exponential constant, K_{inc_0}, and the activation energy con-

stant, E_A.

The method for deriving the new temperature set-point in this case is the solution of a pair of simultaneous equation with two unknowns. As above, the adaptation procedure only considers the current growth rate value and the previous calculation. Hence, using the current growth rate and temperature measurements, T_1 and G_1, and the previous measurements, T_2 and G_2, the two unknowns, K_{inc_0} and E_A are calculated using

$$G_1 = NK_{inc_0}e^{\frac{-E_{inc}}{RT_1}} \tag{4.4}$$

$$G_2 = NK_{inc_0}e^{\frac{-E_{inc}}{RT_2}}. \tag{4.5}$$

Effectively, this method derives a best model fit of the system, limited only by the accuracy of the temperature and thickness measurements.

4.4 Simulations

Before implementation, each of the above described controllers were first simulated using Simulink[1]. The objective of the simulations was to help design an outer loop controller for our system conditions. To facilitate this, we explored the performance of the controllers while simulating run conditions. These conditions include

- *Delay in Measurements:* As described in chapter 2, the EFTIR thickness measurements are computer only every 45 seconds. This presents a limitation on the speed of the outer loop to perceive deviations from the optimum and act to correct it.

- *Quantization of sampled data:* In measuring and computing the thickness measurements, the software truncates the output to an accuracy correct to 100 Å.

[1] A package within Matlab ©, produced by The MathWorks, Inc. (24 Prime Park Way, Nattick, Mass. 01760)

- *Noise:* System and measurement noise are both present in this controller. There is measurement noise associated with the EFTIR and temperature sensors which needs to be included in the simulation. Additionally, system noise and drift are present.

The controllers were evaluated on their stability, robustness and ability to hit the target growth rate. In modeling the actual system, the extensive model developed in chapter 2 was employed. This model is a function of pressure and temperature. To simulate the system behaviour, system noise was added to the model parameters as shown in Appendix B.

In all the simulations presented below, the PID controller designed in chapter 3 is used as the temperature controller. Additionally, the control voltage to the system is not limited to 2.7 V as it is in the real system. It is allowed to operate at any voltage. The result of this is that the time for the temperature to reach set-point is greatly reduced from $\approx$ 45 seconds to less than 5 seconds. This effectively allows the outer loop simulation to be faster in our simulations. Hence instead of the outer-loop model control command being updated every 45 seconds, in our simulations, it is updated every 5 seconds. Additionally, to simply investigate the simulated performance of the different algorithms, the simulations were performed without quantization in the thickness measurements. The effects of quantization are considered later.

4.4.1 Linearised Model Update

Figure 4-4 shows the block diagram used to simulate our controller. This diagram depicts the flow of signals for the type I updating as discussed above.

The desired growth rate is fed into our simplified model which generates the desired temperature set-point. The temperature is added to ΔT and supplied to the Temperature Loop block. This loop simulates the inner PID controlled temperature loop described in chapter 3. The Temperature Loop output, which corresponds to the controlled temperature, is supplied to the Growth block. This block consists of the extensive model of epitaxial deposition process. The Growth block generates

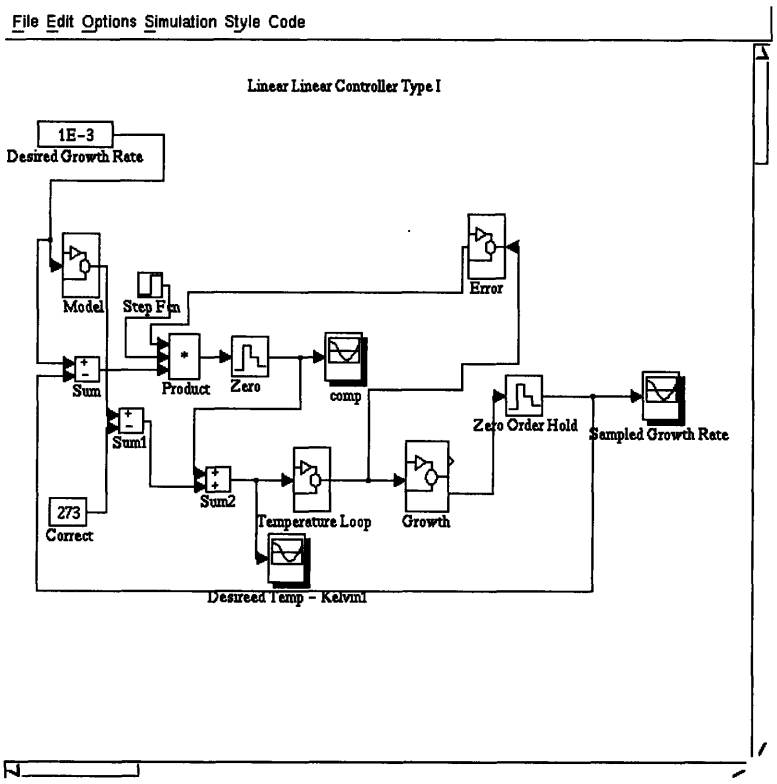

Figure 4-4: The Block Diagram for Type I System

a growth rate value which is sampled and fed back to be periodically compared to our desired growth rate, generating ΔG. The Error block's input is the current temperature. Using this value, it calculates the linearised curve of the model at the point of operation, $\frac{\partial T}{\partial G}$. This value multiplied by ΔG is ΔT. The block details for the Growth and Temperature loop blocks are presented in Appendix B.

Figures 4-5, 4-6 and 4-7 show the results of the simulations using the linear method type I with a desired growth rate of 1×10^{-3} microns/minute at 1 milliTorr. As can be seen from Figure 4-7 the growth rate using this method never actually reaches the desired value of 1×10^{-3} microns/minute. There is a steady state error which results from the linear approximation of an exponential system. In the case of the type 0 system, whose structure is shown in Figure 4-8 , there is still a steady state error associated with the growth rate. Figures 4-9, 4-10, and 4-11 are simulated results using this structure.

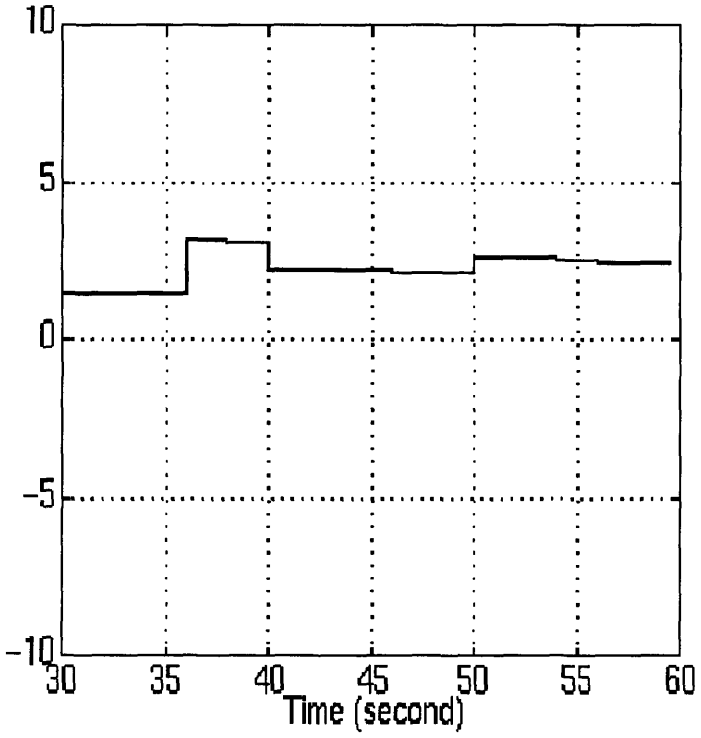

Figure 4-5: Linear type I simulations - ΔT

4.4.2 Adaptive Controller - Pre-exponential

The simulation structure used in Simulab for this algorithm is shown in Figure 4-12. The Error block in the figure calculates takes in the current temperature from the Temperature Loop and the growth rate and calculates the new pre-exponential constant K_{inc_o}. This value is fed, along with the desired growth rate, to the growth model block which calculates the new temperature set point based on (4.1).

Figure 4-13 shows the temperature set-point supplied to the inner control loop during operation. Figure 4-14 shows the sampled growth rate as would be calculated from EFTIR readings. Figure 4-15 shows the values of the adapted pre-exponential parameter during the run. The figures show that this system is able to attain the target growth rate given our simulated system.

4.4.3 Adaptive Controller - Pre-exponential and Activation Energy

Figure 4-16 shows the simulation structure for this control process. In this mode, the Error block takes in the temperature and growth rate measurements for two different points in time. Using these measurements, a simultaneous solution of our simplified model is solved to calculate the pre-exponential (K_{inc_o}) and the activation energy (E_{inc}) parameters for our model. These new parameters are inputs into the Model block which calculates, based upon our new model and desired growth rate, a temperature set-point input for our inner loop.

Figures 4-17 and 4-18 show the activation energy and pre-exponential constants respectively during a simulated run. Figure 4-20 shows the corresponding temperature set-point supplied to the inner loop, and Figure 4-19 shows the corresponding growth rate. These figures show the initial ramp up to steady state operation.

These simulations show that this method can effectively be used to control our system. In the steady state, we are able to attain the target growth rate. This method, however, is very sensitive as compared to the other methods because its parameters are determined from only two measurement points. This may lead to undesired fluctuations of the parameters as our system reacts to measurement and system noise. One method of overcoming this problem would be to use a weighted moving average approach.

4.5 Quantization

As stated above, the existence of quantization in thickness and time of our measuring systems places severe limitations on the actual implementation. The current system for measurement of EFTIR samples is accurate to two decimal places (100 Å). In the time domain, we are limited to a sampling time of 40–45 seconds. The effect of this, coupled with the presence of measurement noise, is to limit our ability to accurately ascertain the growth rate of the system from the *in-situ* measurements during the

run.

For the temperature and pressure regime being considered, we expect a growth rate of from approximately 8.5×10^{-4} microns/minute (600°C) to 2.7×10^{-3} microns/minute (650°C). Because of quantization uncertainty, a measured step change of 0.02 microns in 12 minutes (16 × 45 second steps) could correspond to a growth rate of any where from 8.3×10^{-4} to 2.5×10^{-3} microns/minute.

One solution to this problem, given current instruments, is to lengthen the number of samples between calculation of growth rate and eventual command to the inner loop. However this is precisely the problem we are trying to solve: we want to minimize the time at an undesired growth rate. This could also lead to instability as the outer loop tends to over-compensate.

Another solution is to improve both the sample time and the number of significant digits available from the EFTIR measurements. One more digit in EFTIR measurements would improve accuracy of growth rate estimates for a .020 micron step in 12 samples to a range of 1.583×10^{-3} microns/minute to 1.75×10^{-3} microns/minute.

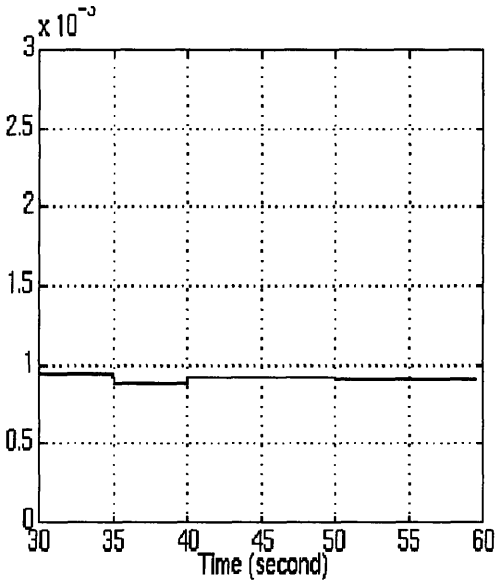

Figure 4-6: Linear type I simulations - growth rate (microns/minute)

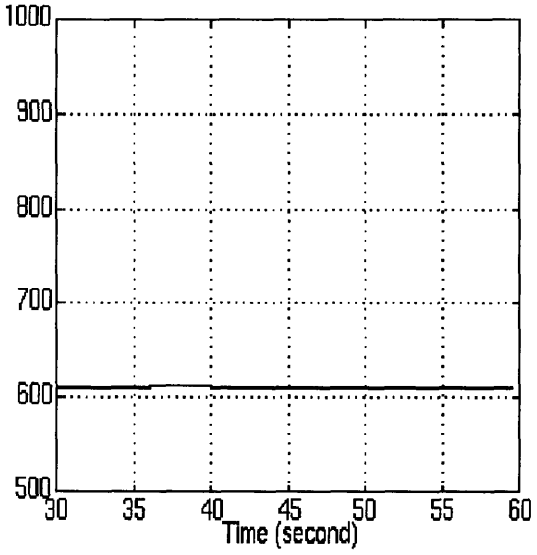

Figure 4-7: Linear type I simulations - desired temperature (°C).

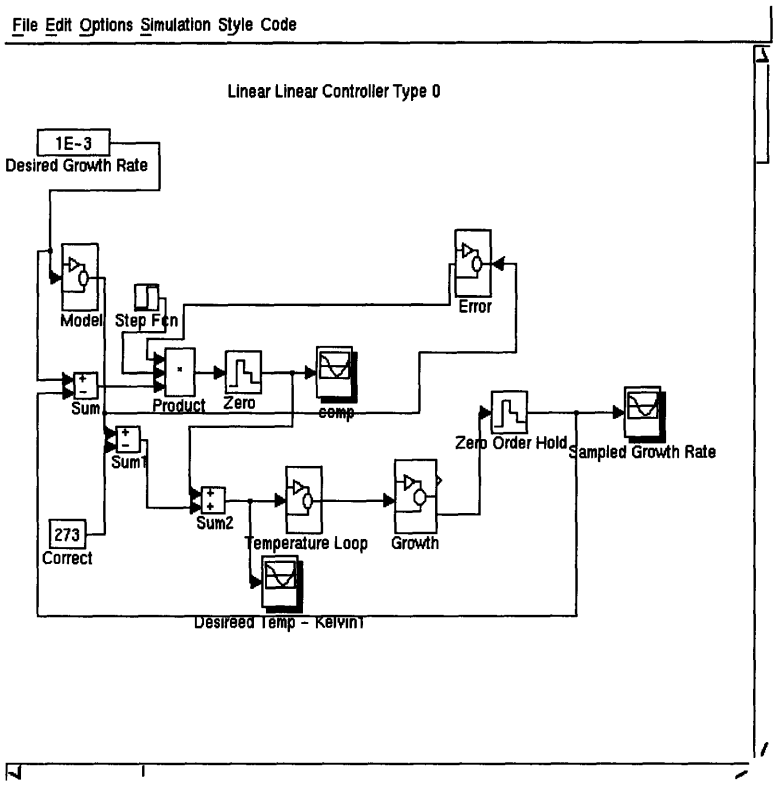

Figure 4-8: Linear type 0 simulation block diagram

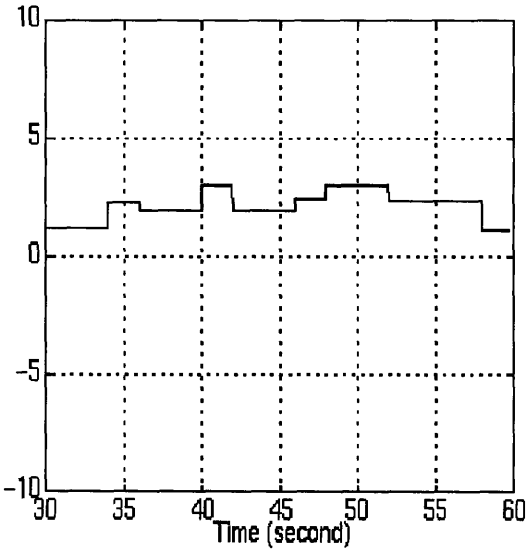

Figure 4-9: Linear type 0 simulations - ΔT.

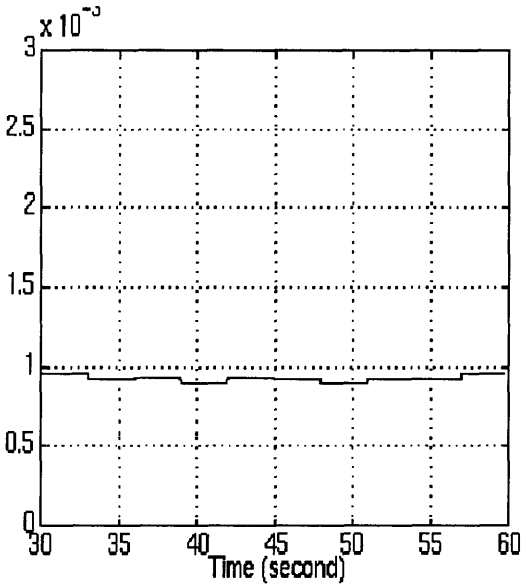

Figure 4-10: Linear type 0 simulations - growth rate (microns/minutes).

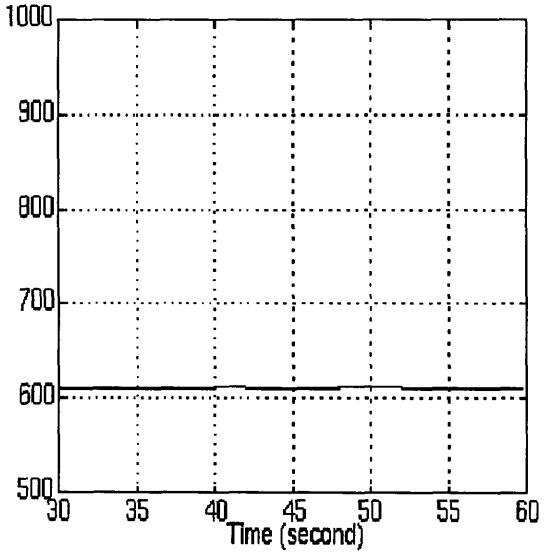

Figure 4-11: Linear type 0 simulations - desired temperature (^{o}C).

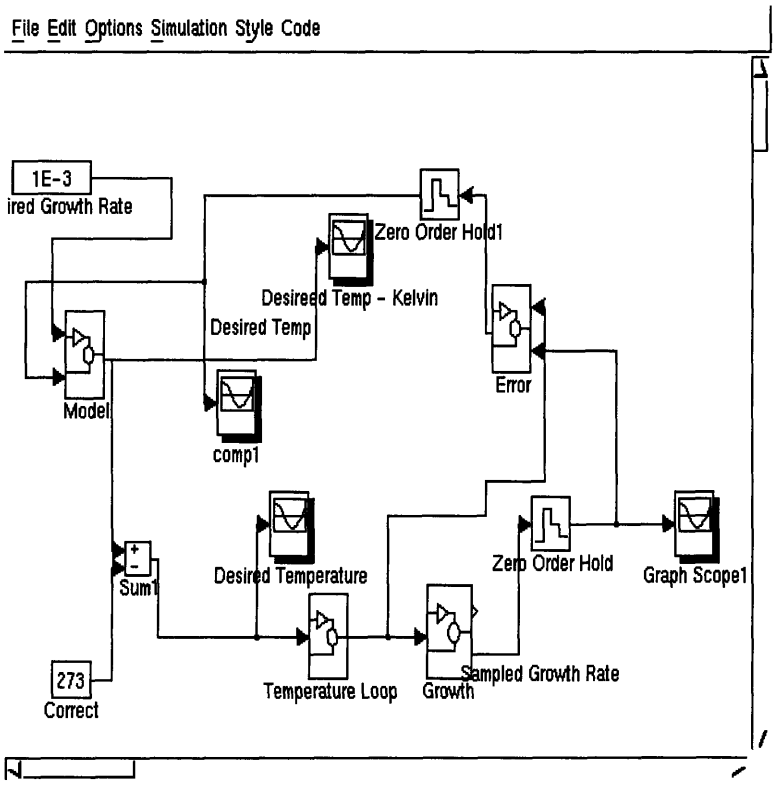

Figure 4-12: The adaptive controller simulation structure - pre-exp.

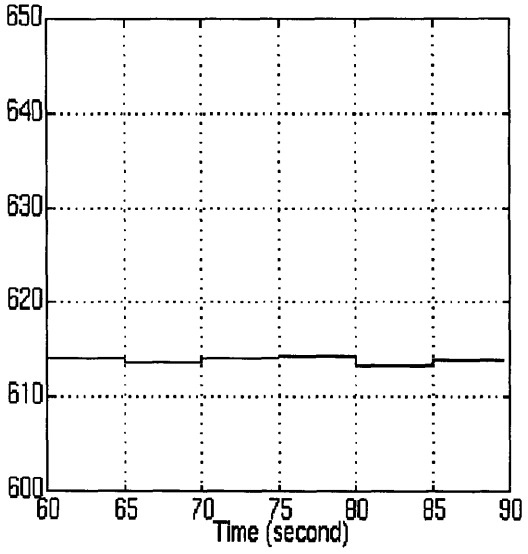

Figure 4-13: Adaptive pre-exp. simulations - temperature set-point (°C).

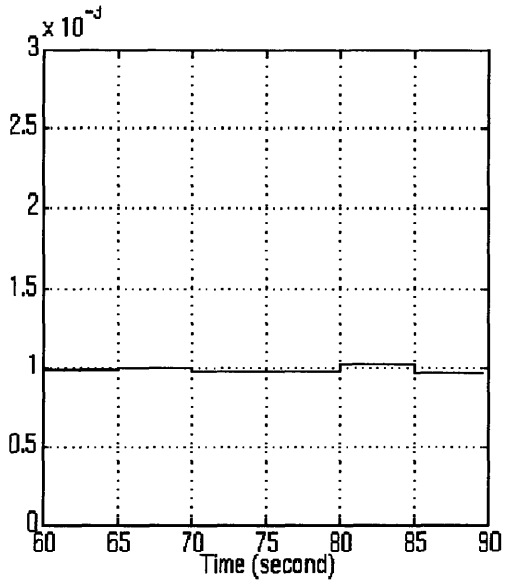

Figure 4-14: Adaptive pre-exp. simulations - growth rate (microns/minute).

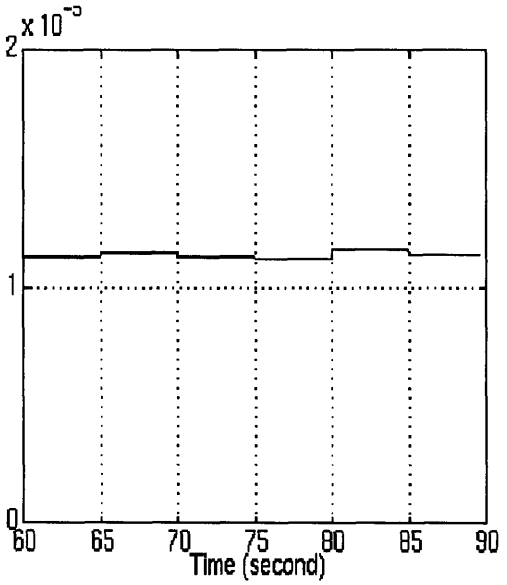

Figure 4-15: Adaptive Pre-exp. simulations - the pre-exponential coefficient.

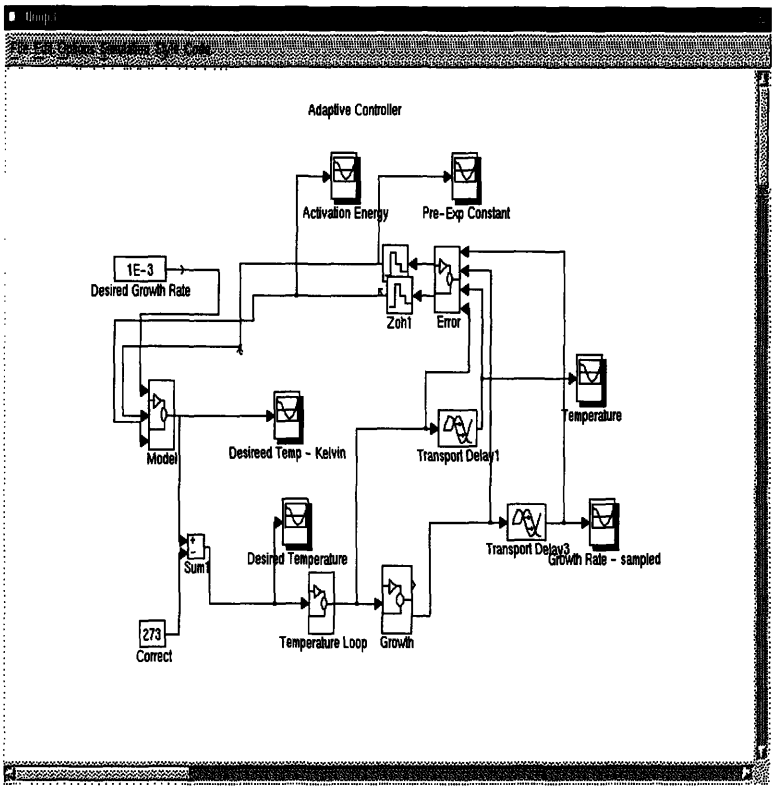

Figure 4-16: Simulation structure for adaptive control of pre-exp. and activation energy parameters.

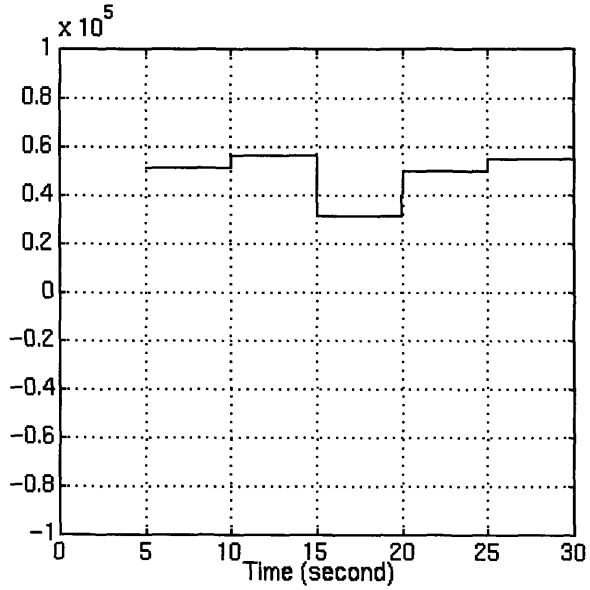

Figure 4-17: Values for activation energy parameter during adaptive control simulation (cal/mole).

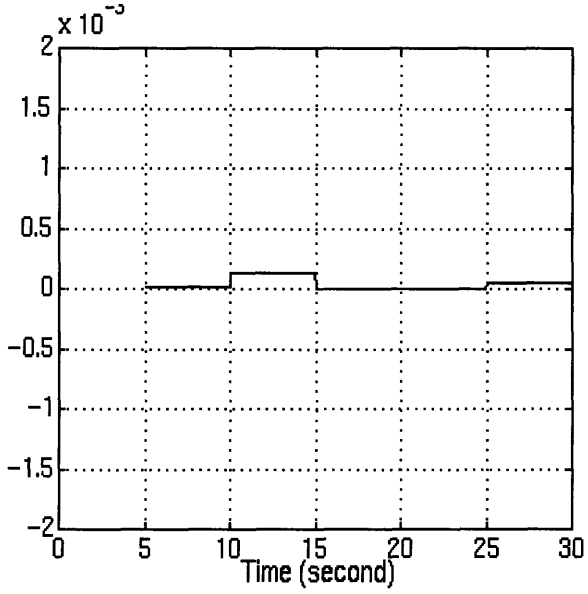

Figure 4-18: Values for pre-exponential parameter during adaptive control simulation.

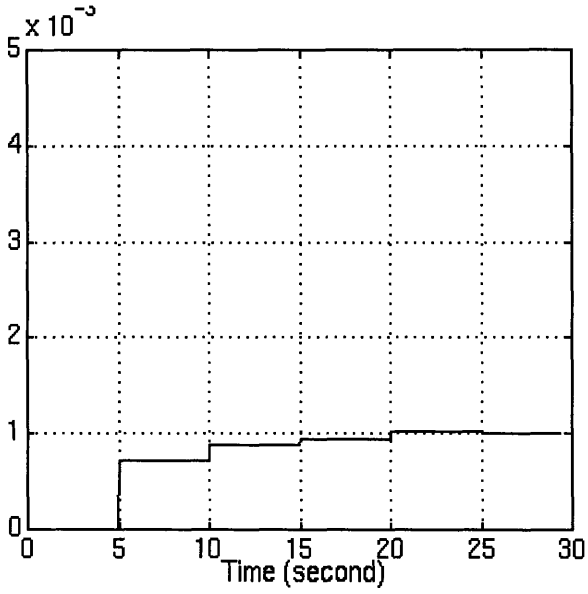

Figure 4-19: Growth rate of system during adaptive controlled simulation (microns/minute).

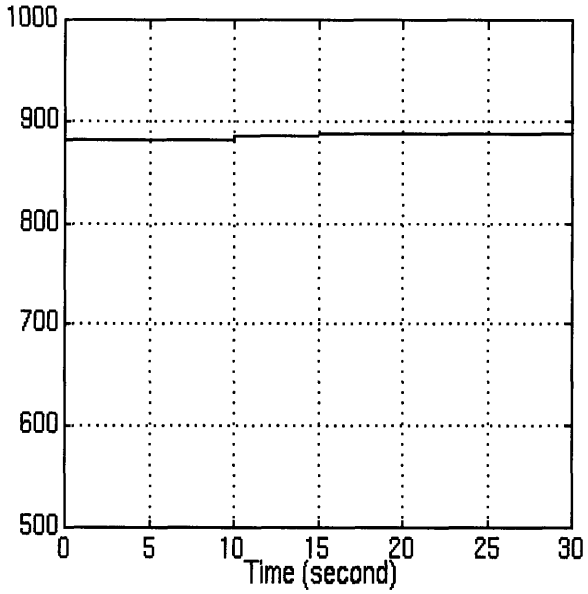

Figure 4-20: Temperature set-point to inner loop during adaptive controlled simulations (K).

Chapter 5

Conclusion

5.1 Summary

The primary objective of this thesis was to investigate an approach for controlling the growth rate of an epitaxial silicon process. Our work concentrated on a specific regime of epitaxial growth: low pressure ($<$ 3 milliTorr) and low temperature ($<$ 650°C). Using these constraints, we develop a simplified model of epitaxial growth which is primarily temperature dependent. Experimental and reported results confirm that for LPCVD of silicon this conclusion is valid.

This thesis presents a hierarchical control structure which can be used to control LPCVD of silicon. The structure consists of two main loops. The inner loop controls the temperature of the reactor to a externally determined set-point. For our work and system, we developed a digital PID compensated feedback controller for this loop. The second loop is a model based controller which uses EFTIR measurements to adjust model parameters. Using this new updated model, our controller determines the new set-point for the inner loop.

There are several advantages to our control structure. The use of a model based system allows for a more flexible and potentially accurate controller. The model can be extended and refined as more information is gathered about the reactor. For example, the effects of flowrate or wafer orientation can be added to the model with little difficulty. The controller is also portable to different regimes of operation. For

a regime which is temperature and pressure dependent, for example, a change in the model and the implementation of a control loop to control the system pressure based upon an externally determined set-point would be the only necessary additional component necessary. The rest of the original structure would remain unchanged.

The time and thickness quantization in our case presents a fundamental limitation in the determination of the actual growth rate of the system in real time. This problem thereby limits our ability to accurately determine the required temperature set-point and implicitly, control the growth rate. Simulations show that this problem can be addressed by improvements in measurement accuracy.

5.2 Future Work

There are several avenues of research that should be pursued in this field to improve control of silicon epitaxial processes.

- An investigation into the design and implementation of a multi-variable inner controller. This controller should regulate the temperature, pressure and flow rate of the reactor. Monitoring and actuation of these three coupled parameters would allow more complete control of the system.

- Improvement in sensor accuracy and error reduction. As mentioned before, the EFTIR measuring tool places a limitation on the overall speed of the outer thickness control loop. Improvement of the time for the system to measure and calculate the thickness is essential.

- Incorporation of the controller into a comprehensive control system, including integration with a run-by-run controller. In this scenario, the run-by-run "loop" would update the model parameters on a wafer to wafer basis.

- An investigation into the sensoring and control of uniformity accross the wafer surface.

Appendix A

The Kalman Filter

The following outlines the Kalman filter model designed for optimal estimation of the surface temperature during deposition. As described in chapter 3, our temperature measurements from the optical sensor were distributed around a mean value in a Gaussian fashion. The aim of our filter was to determine a best estimate of the actual temperature given the Gaussian noise.

A.0.1 The system

The process model is assumed to be of the form

$$x_k = x_{k-1} + \Lambda_{k-1} u_{k-1} + w_{k-1} \tag{A.1}$$

where x_k represents the current state temperature, w_k represents the system noise and u_k is a deterministic input with a scaling factor Λ_k. The system noise, w_k is assumed to be Gaussian with a zero (0) average and a standard deviation of Q_k. The deterministic input, u_k, in this case is the driving voltage to the power supplier to the heater of the system which is controlled externally. The scaling factor is our model based temperature value derived from our observed temperature characteristics of the system.

For our system

$$\Lambda_{k-1} u_{k-1} = V \times \frac{HG}{1 + HG} \tag{A.2}$$

Where H and G are the system and compensator system functions respectively.

The measurement model for our process is assumed to be of the form

$$z_k = x_k + v_k \tag{A.3}$$

where z_k is the measured temperature. The measurement error v_k is assumed to be Gaussian with a mean of zero (0) and a standard deviation of R_k.

A.0.2 The Filter

The initial conditions for the filter are that the initial estimate of the layer thickness, $\hat{x}_0 = E[x(0)]$. This quantity would be measured by taking several measurements of the stationary system. The initial covariance (standard deviation in this case) is

$$P_0 = E[(x(0) - \hat{x}_0)^2] \tag{A.4}$$

The estimate of the temperature is defined by the following equation.

$$\hat{x}_k = \hat{x}_{k-1} + \Lambda_{k-1}u_{k-1} + K_k[z_k - \hat{x}_{k-1} - \Lambda_{k-1}u_{k-1}] \tag{A.5}$$

K_k is the Kalman gain matrix which is updated every state.

$$K_k = \frac{P_k(-)}{P_k(-) + R_k} \tag{A.6}$$

where

$$P_k(-) = P_{k-1} + Q_{k-1} \tag{A.7}$$

and

$$P_k(+) = [1 - K_k]P_k(-) \tag{A.8}$$

Equations A.6 to A.8 update the Kalman gain matrix (which is a gain factor in this one dimensional case) after each state.

The standard deviations for the system and measurement noise are assumed to be constant throughout.

Appendix B

Simulation Blocks

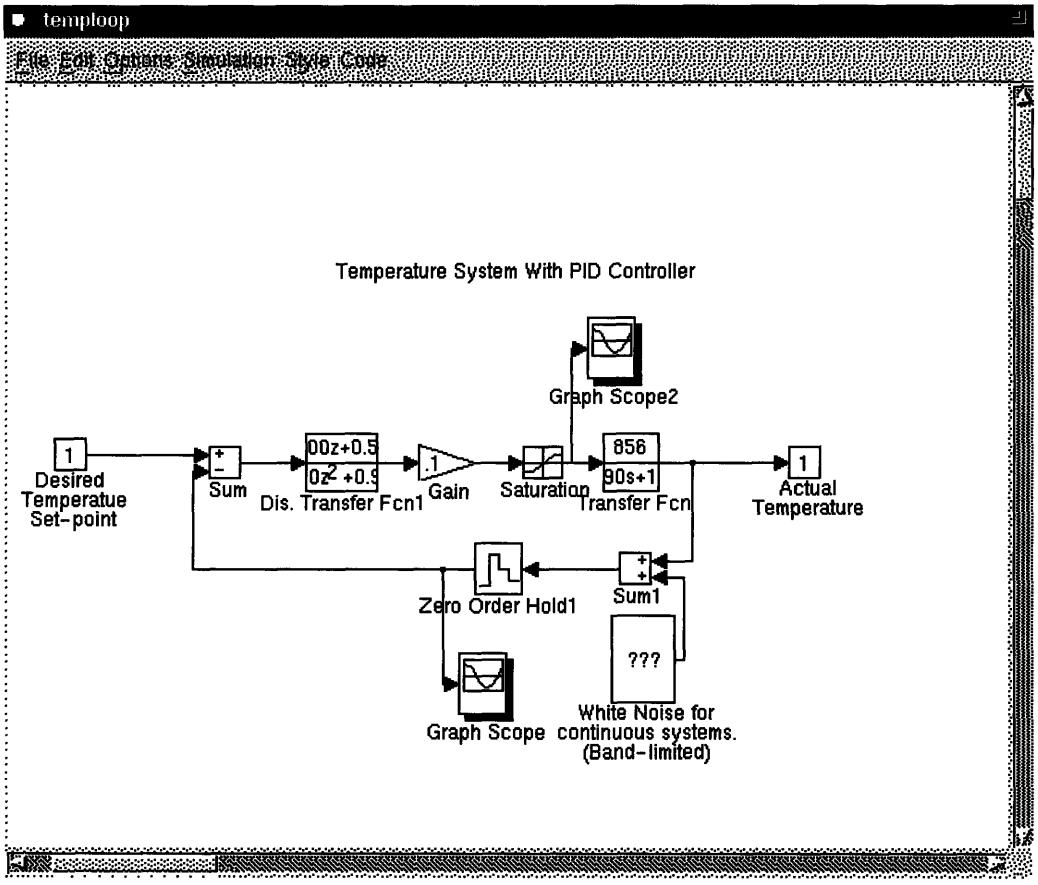

Figure B-1: Inner temperature toop block for outer loop simulations.

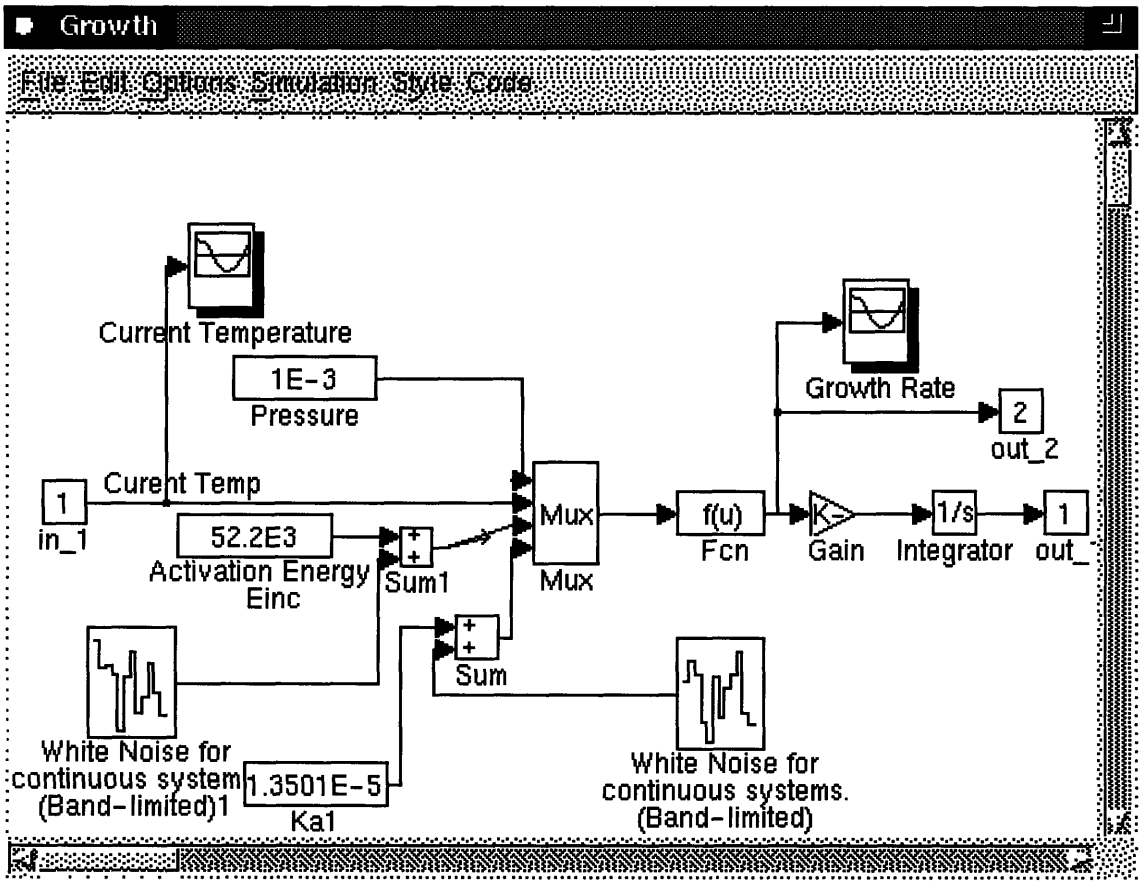

Figure B-2: Growth model for outer loop simulations.

Appendix C

Controller interface

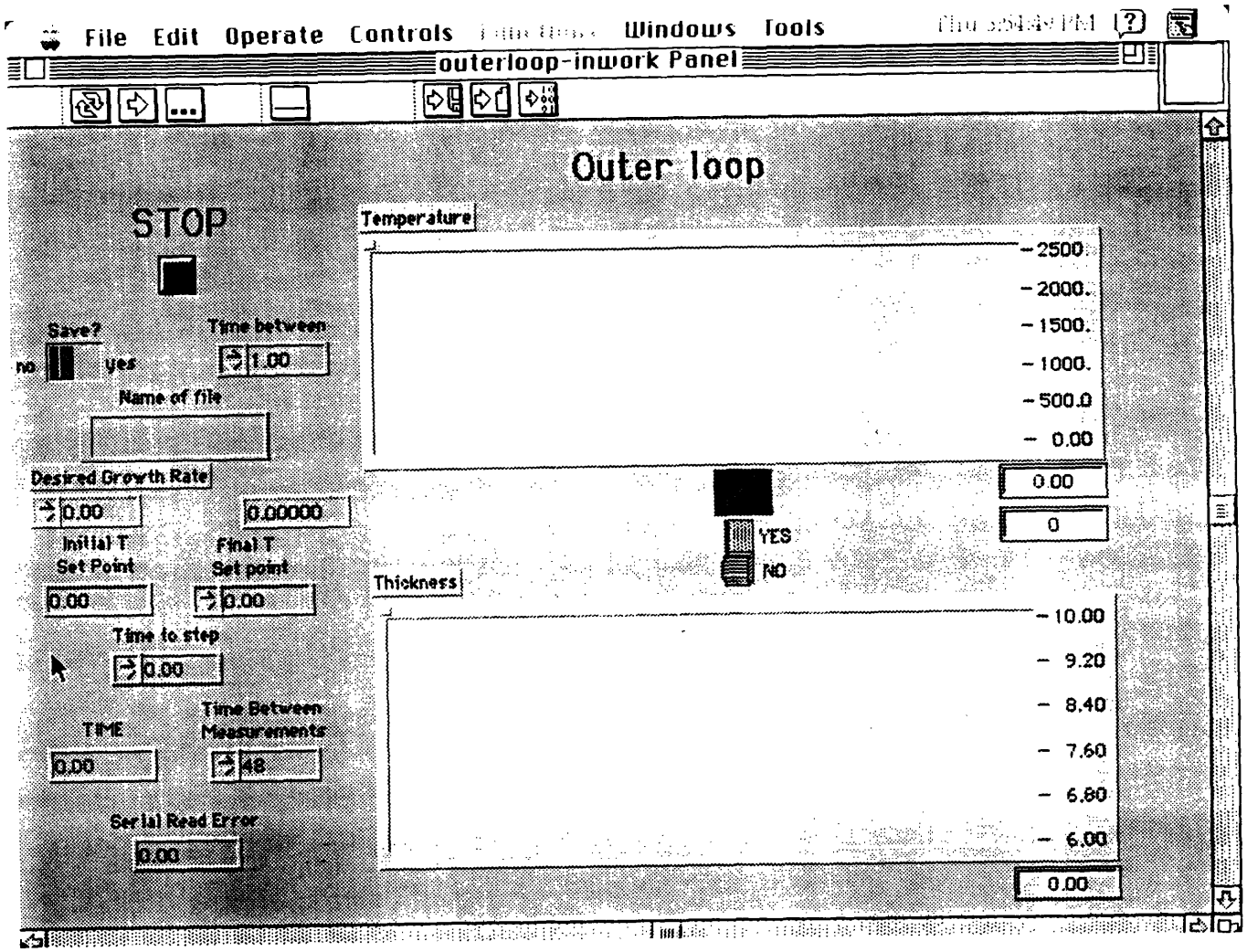

Appendix D

Hardware Setup (UHV Reactor and Computer Controller)

Bibliography

[1] Z. Zhou, F. Yu, and R. Reif, "A multichamber single-wafer chemical vapor deposition reactor and electron cyclotron resonance plasma for flexible integrated circuit manufacturing," *J. Vac. Sci. Technol.*, 1991.

[2] D. Greve and M. Racanell, "Growth Rate of Doped and Undoped Silicon by UHV/CVD," 1990.

[3] K. Sinniah, "New Mechanism for Hydrogen Desorption from Covalent Surfaces: The Monohydride Phase on Si(100)," *Physical Review Letters*, 1989.

[4] Z. Zhou, "Thickness measurements using LP UHV CVD reactor," 1993.

[5] J. Comfort and R. Reif, "Chemical Vapor Deposition of Espitaxial Silicon," tech. rep., MIT VLSI Memo No. 88-460, 1988.

[6] *SDCR-B Series 2700-Watt Power Supplies: Instruction Manual.* Sorensen Company, 5555 North Elston Ave. Chicago, IL 60630, 1992.

[7] F. Yu, Z. h. Zhou, P. Stout, and R. Reif, "*In-Situ* monitoring for Epitaxial Film Thickness by IEMI," *IEEE Transactions on Semiconductor Manufacturing*, vol. 5, no. 1, Feb. 1992.

[8] T. Carroll and W. F. Ramirez, "Optimal Control of Positive Optical Photoresist Develpment," *SPIE - Integrated Circuit Metrology, Inspection and Process Control V*, 1991.

[9] S. Gates and S. Kulkarni, "Hydrogen coverage during Si growth from SiH_4 and Si_2H_4," *Appl. Phys. Lett.*, 1992.

[10] S. K. S.M. Gates, C.M. Greenlief and H. Sawin, "Surface reactions in Si chemical vapor deposition from silane," *J. Vac. Sci Technol.*, vol. A8, p. 2965, 1990.

[11] Z. Zhou, I. Yang, F. Yu, and R. Reif, "Fundamental of epitaxial silicon film thickness measurements using emission and reflection Fourier transform infrared spectroscopy," *J. Appl. Phys*, 1993.

[12] K. Jensen and S. Vardeman, "Optimal Adjustment in the Presence of Deterministic Process Drift and Random Adjustment Error," *Technometrics*, vol. 35, no. 4, Nov. 1993.

[13] E. Sachs, R.-S. Guo, S. Ha, and A. Hu, "Process Control System for VLSI Fabrication," *IEEE Transactions on Semiconductor Manufacturing*, vol. 4, no. 2, May 1991.

[14] R. Guo and E. Sachs, "Modeling, Optimization and Control of Spatial Uniformity in Manufacturing Processes," *IEEE Transactions on Semiconductor Manufacturing*, vol. 6, no. 1, pp. 46–57, 1993.

[15] O. Marenzi, "Control of Epitaxial film thickness," Master's Thesis, Mass. Inst. of Tech., 1993.

[16] W. M. Duncan, S. A. Henck, and L. M. Loewenstein, "Spectral Ellipsometry for *In-Situ* Real-Time Measurement and Control," tech. rep., Central Research Laboratories and Semiconductor Process and Design Center, TI Inc, Dallas, Texas 75265, 1992.

[17] A. Gelb, ed., *Applied Optimal Estimation.* The MIT Press, 1984.

[18] K. J. Astrom and B. Wittenmark, *Computer-Controlled Systems: Theory and Design.* Prentice-Hill, Inc, 1990.

[19] T. Carroll and W. F. Ramirez, "On-line state and model parameter identification of the positive optical photoresist development process," *AIChE*, vol. 36, no. 7, pp. 1046–1053, 1990.